

Using Josephson junctions to determine the pairing state of superconductors without crystal inversion symmetry

K. Børkje¹

¹*Department of Physics, Norwegian University of Science and Technology, N-7491 Trondheim, Norway*
(Dated: October 26, 2018)

Theoretical studies of a planar tunnel junction between two superconductors with antisymmetric spin-orbit coupling are presented. The half-space Green's function for such a superconductor is determined. This is then used to derive expressions for the dissipative current and the Josephson current of the junction. Numerical results are presented in the case of the Rashba spin-orbit coupling, relevant to the much studied compound CePt₃Si. Current-voltage diagrams, differential conductance and the critical Josephson current are presented for different crystallographic orientations and different weights of singlet and triplet components of the pairing state. The main conclusion is that Josephson junctions with different crystallographic orientations may provide a direct connection between unconventional pairing in superconductors of this kind and the absence of inversion symmetry in the crystal.

PACS numbers:

I. INTRODUCTION

The question of how parity violation affects superconductivity has until recently not been subject to much experimental studies. In recent years, however, superconductivity has been discovered in several materials with a noncentrosymmetric crystal structure. This offers an arena for the study of superconductivity in the absence of inversion symmetry. Theoretical studies of such systems have predicted several exotic features, reviewed in Refs. 1 and 2. The absence of inversion symmetry allows an antisymmetric spin-orbit coupling in the Hamiltonian. This has, among other things, the consequence that the pairing state of the superconductor may not be classified as a spin singlet or a spin triplet state.^{3,4}

The most famous and studied example of the noncentrosymmetric superconductors is the heavy fermion compound CePt₃Si, which possess several interesting properties.^{1,2,5,6} For instance, the pairing state of CePt₃Si seems to contain line nodes⁵ even though NMR measurements are of the kind expected for a conventional superconductor.⁶ Several theories have been put forward to explain this.^{7,8,9} Other examples of noncentrosymmetric superconductors are UIr, Li₂Pd₃B, Li₂Pt₃B, Cd₂Re₂O₇ and possibly KOs₂O₆. The absence of inversion symmetry in these materials destroys spin degeneracy through antisymmetric spin-orbit coupling. This is expected to be strong in some of the materials mentioned above,^{10,11} especially in compounds containing atoms with a large atomic number. Line nodes also seem to appear in the pairing state of Li₂Pt₃B,^{12,13} whereas Cd₂Re₂O₇, Li₂Pd₃B and KOs₂O₆ appear to be nodeless.^{12,14,15}

The experiments performed on these materials so far mostly concern quantities such as specific heat, magnetic penetration depth and the nuclear spin-lattice relaxation rate. They are all important in order to determine the pairing state of a superconductor. However, tunneling spectroscopy and experiments on Josephson junctions are

also a very useful tool in this respect, both in conventional and high- T_c superconductors.^{16,17,18}

Recently, theoretical studies of transport in a junction between a normal metal and a noncentrosymmetric superconductor were performed.^{19,20} These kind of transport measurements do not probe bulk properties directly, but will depend on how the pairing state is affected by the surface. Due to the possible triplet component, one may expect the gap to deviate from its bulk value^{21,22} and formation of Andreev bound states near the surface.^{17,23}

The transport properties of a Josephson junction consisting of two noncentrosymmetric superconductors have been investigated in Ref. 24. Given particular pairing states, it was noted that both the quasiparticle current and the critical Josephson current would depend on the relative crystal orientation of the superconductors. Similar effects may appear with the two-band superconductor MgB₂.^{25,26} However, in Ref. 24, the bulk density of states was used, neglecting the effect of surface scattering. One might therefore question the validity of these results, since the effect of surface reflection was not considered.

In this paper, the effect of surface scattering is taken into account when determining the transport properties of the above mentioned Josephson junction. It is shown that the effects predicted in Ref. 24 may still appear, even though the surface provides a strong coupling between the spin-orbit split bands. Thus, in some cases one may expect qualitative changes in the differential conductance for different relative crystal orientations of the two superconductors. In addition, quantitative changes in the critical Josephson current may be expected. This could make it easier to establish a direct connection between the unconventional pairing and the absence of inversion symmetry. This paper is hence an attempt to motivate experimental work on such junctions.

The paper is organized as follows. In section II, we define the model containing a general antisymmetric spin-orbit coupling. The Green's function is then established,

first in the bulk case and then in a half-space or semi-infinite scenario. Expressions for the tunneling currents are presented in section III. In section IV, numerical results using the Rashba spin-orbit coupling are presented to exemplify the predicted effects.

II. MODEL

We will start by considering the bulk properties of a clean superconductor with spin-orbit split bands. The model will be written down in the continuum limit. Having established the bulk Green's function, we move on to derive the Green's function in the presence of a reflecting surface.

A. Bulk properties

Let the Hamiltonian consist of two terms, $H = H_N + H_{SC}$, a normal part and a part describing superconductivity. In the bulk, the normal part is

$$H_N = \int d\mathbf{k} \phi_{\mathbf{k}}^\dagger [(\varepsilon_{\mathbf{k}} - \mu)\mathbb{1} + \mathbf{B}_{\mathbf{k}} \cdot \boldsymbol{\sigma}] \phi_{\mathbf{k}}, \quad (1)$$

where $\phi_{\mathbf{k}}^\dagger = (c_{\mathbf{k}\uparrow}^\dagger, c_{\mathbf{k}\downarrow}^\dagger)$, $\varepsilon_{\mathbf{k}}$ is the band dispersion and μ the chemical potential. The vector $\boldsymbol{\sigma}$ consists of the three Pauli matrices.

The vector $\mathbf{B}_{\mathbf{k}}$ describes the anti-symmetric spin-orbit coupling. It removes the spin degeneracy from the band $\varepsilon_{\mathbf{k}}$. The absence of inversion symmetry is reflected in the property $\mathbf{B}_{-\mathbf{k}} = -\mathbf{B}_{\mathbf{k}}$. An electron in a state with momentum \mathbf{k} will align its spin parallel or antiparallel to $\mathbf{B}_{\mathbf{k}}$. The symmetries of $\mathbf{B}_{\mathbf{k}}$ may be determined from point group symmetry considerations.²⁷

Diagonalization of equation (1) gives $H_N = \sum_{\lambda=\pm, \mathbf{k}} \xi_{\lambda, \mathbf{k}} \tilde{c}_{\lambda, \mathbf{k}}^\dagger \tilde{c}_{\lambda, \mathbf{k}}$, where $\xi_{\pm, \mathbf{k}} = \varepsilon_{\mathbf{k}} - \mu \pm |\mathbf{B}_{\mathbf{k}}|$. The spin of an electron in a state with momentum \mathbf{k} will point parallel(antiparallel) to $\mathbf{B}_{\mathbf{k}}$ in band $+$ ($-$).

We write down the term responsible for superconductivity in terms of the long-lived excitations in the normal state, *i.e.*

$$H_{SC} = \frac{1}{2} \sum_{\lambda\mu} \int d\mathbf{k} d\mathbf{k}' V_{\lambda\mu}(\mathbf{k}, \mathbf{k}') \tilde{c}_{\lambda, -\mathbf{k}}^\dagger \tilde{c}_{\lambda, \mathbf{k}}^\dagger \tilde{c}_{\mu, \mathbf{k}'} \tilde{c}_{\mu, -\mathbf{k}'}. \quad (2)$$

We will consider the limit where the spin-orbit splitting is much larger than the superconducting gaps. This is a relevant limit, at least for the materials CePt₃Si¹⁰ and Cd₂Re₂O₇.¹¹ In that case, interband Cooper pairs are strongly suppressed, even though the two bands may touch at some isolated points on the Fermi surface.¹⁰ Thus, the model (2) contains only intraband Cooper pairing. However, it does include an internal Josephson coupling, *i.e.* scattering of Cooper pairs between the bands.

The standard mean field approach gives

$$H_{SC} = \frac{1}{2} \sum_{\lambda} \int d\mathbf{k} \left(\tilde{\Delta}_{\lambda, \mathbf{k}} \tilde{c}_{\lambda, \mathbf{k}}^\dagger \tilde{c}_{\lambda, -\mathbf{k}}^\dagger + \tilde{\Delta}_{\lambda, \mathbf{k}}^* \tilde{c}_{\lambda, -\mathbf{k}} \tilde{c}_{\lambda, \mathbf{k}} \right) \quad (3)$$

where $\tilde{\Delta}_{\lambda, \mathbf{k}} = -\sum_{\mu} \int d\mathbf{k}' V_{\lambda\mu}(\mathbf{k}, \mathbf{k}') \langle \tilde{c}_{\mu, \mathbf{k}'} \tilde{c}_{\mu, -\mathbf{k}'} \rangle$. $\tilde{\Delta}_{\lambda, -\mathbf{k}} = -\tilde{\Delta}_{\lambda, \mathbf{k}}$ follows from the fermionic anticommutation relations. One should note that the two bands are decoupled in the mean field approximation. However, the gaps $\tilde{\Delta}_{\pm, \mathbf{k}}$ are in general not independent, but related through the self-consistency equations due to the above mentioned possibility of interband pair scattering.²⁸

Let \mathcal{K} denote the time-reversal operator, whose effect on the operators in the spin basis is $\mathcal{K} : c_{\mathbf{k}, \sigma}^\dagger = -\sigma c_{-\mathbf{k}, -\sigma}^\dagger$. It may be derived that $\mathcal{K} : \tilde{c}_{\lambda, \mathbf{k}}^\dagger = t_{\lambda, \mathbf{k}} \tilde{c}_{\lambda, -\mathbf{k}}^\dagger$, where $t_{\lambda, \mathbf{k}} = -t_{\lambda, -\mathbf{k}}$ is a gauge-dependent phase factor. One may write $\tilde{\Delta}_{\lambda, \mathbf{k}} = t_{\lambda, \mathbf{k}} \chi_{\lambda, \mathbf{k}}$, where $\chi_{\lambda, \mathbf{k}}$ is the order parameter for pairs of time reversed states on which observable quantities will depend. Thus, $\chi_{\lambda, \mathbf{k}} = \chi_{\lambda, -\mathbf{k}}$ may be expanded in terms of even basis functions of irreducible representations of the space group.²⁹

Define the matrix $\Delta_{\mathbf{k}}$ whose elements are the gap functions $\Delta_{\mathbf{k}, \sigma\sigma'}$ in a spin basis. By transforming equation (3), one arrives at

$$\Delta_{\mathbf{k}} = \eta_{\mathbf{k}, S} (-i\sigma_y) + \eta_{\mathbf{k}, T} (\hat{\mathbf{B}}_{\mathbf{k}} \cdot \boldsymbol{\sigma}) (-i\sigma_y). \quad (4)$$

Thus, in the absence of spatial inversion symmetry, the order parameter in a spin basis have no definite parity, but is in general a linear combination of a singlet (S) and a triplet (T) part.^{3,4,8,30} The singlet and triplet components are determined by

$$\begin{aligned} \eta_{\mathbf{k}, S} &= \frac{1}{2} (\chi_{+, \mathbf{k}} + \chi_{-, \mathbf{k}}), \\ \eta_{\mathbf{k}, T} &= \frac{1}{2} (\chi_{+, \mathbf{k}} - \chi_{-, \mathbf{k}}). \end{aligned} \quad (5)$$

There is no need to specify the momentum dependence of the gaps $\chi_{\lambda, \mathbf{k}}$ at this point.

In the bulk, the Green's functions are diagonal in momentum space due to translational symmetry. In the imaginary time formalism, define the normal and anomalous Green's functions as $\mathcal{G}_{b, \sigma\sigma'}(\mathbf{k}, \tau) = -\langle T_\tau c_{\mathbf{k}\sigma}(\tau) c_{\mathbf{k}\sigma'}^\dagger(0) \rangle$ and $\mathcal{F}_{b, \sigma\sigma'}(\mathbf{k}, \tau) = \langle T_\tau c_{\mathbf{k}\sigma}(\tau) c_{-\mathbf{k}\sigma'}(0) \rangle$, respectively, where the subscript b denotes bulk. It is convenient to transform to fermionic Matsubara frequencies, $\omega_n = (2n+1)\pi/\beta$, where β is the inverse temperature. The bulk Green's function in spin \times particle-hole space,

$$\mathbf{G}_b(\mathbf{k}, i\omega_n) = \begin{pmatrix} \mathcal{G}_b(\mathbf{k}, i\omega_n) & -\mathcal{F}_b(\mathbf{k}, i\omega_n) \\ -\mathcal{F}_b^\dagger(\mathbf{k}, i\omega_n) & -\mathcal{G}_b^t(-\mathbf{k}, -i\omega_n) \end{pmatrix}, \quad (6)$$

is found by solving the Gor'kov equations (A1) presented in appendix A. The components are matrices in spin

space, given by

$$\begin{aligned}\mathcal{G}_b(\mathbf{k}, i\omega_n) &= \frac{1}{2} \sum_{\lambda=\pm} \sigma_{\hat{\mathbf{B}}_k}^\lambda G_\lambda(\mathbf{k}, i\omega_n), \\ \mathcal{F}_b(\mathbf{k}, i\omega_n) &= -\frac{i}{2} \sum_{\lambda=\pm} \sigma_{\hat{\mathbf{B}}_k}^\lambda \sigma_y F_\lambda(\mathbf{k}, i\omega_n),\end{aligned}\quad (7)$$

in terms of the complex scalar functions

$$\begin{aligned}G_\lambda(\mathbf{k}, i\omega_n) &= -\frac{i\omega_n + \xi_{\lambda, \mathbf{k}}}{\omega_n^2 + \xi_{\lambda, \mathbf{k}}^2 + |\chi_{\lambda, \mathbf{k}}|^2}, \\ F_\lambda(\mathbf{k}, i\omega_n) &= \frac{\chi_{\lambda, \mathbf{k}}}{\omega_n^2 + \xi_{\lambda, \mathbf{k}}^2 + |\chi_{\lambda, \mathbf{k}}|^2},\end{aligned}\quad (8)$$

and the matrices

$$\sigma_{\hat{\mathbf{B}}_k}^\lambda = 1 + \lambda \hat{\mathbf{B}}_k \cdot \boldsymbol{\sigma}.\quad (9)$$

B. Half-space Green's function

The bands $+$ and $-$ defined in the previous section has the property that reversing the direction of an electron's momentum while preserving its spin requires a change of bands. Thus, one would expect that the independence of the bands $+$ and $-$ could be vulnerable to scattering, *e.g.* from impurities. In fact, it has been shown that a small concentration of nonmagnetic impurities does not change the picture of independent bands in the mean field approximation.³¹ A perfectly reflecting surface should however lead to a severe mixing of the bands. This needs to be taken into account when describing transport in heterostructures containing these materials.

The presence of a surface will make the Hamiltonian and the Green's function nondiagonal in momentum space. Still, due to the nature of the spin-orbit coupling, it is convenient to work in a plane wave basis. We will assume that the surface is perfectly smooth. Of course, any real surface will have some roughness, which may

very well modify the results of this paper. However, at least for not too rough surfaces, this model is an appropriate starting point. We will also assume that the surface is spin inactive, *i.e.* nonmagnetic.

Consider the simplest case of a perfectly smooth surface at $x = 0$, such that the electrons are confined to $x < 0$. We seek the Green's function $\mathbb{G}(\mathbf{k}_1, \mathbf{k}_2, \tau)$, whose elements are

$$\begin{aligned}\mathcal{G}_{\sigma\sigma'}(\mathbf{k}_1, \mathbf{k}_2, \tau) &\equiv -\langle T_\tau c_{\mathbf{k}_1, \sigma}(\tau) c_{\mathbf{k}_2, \sigma'}^\dagger(0) \rangle, \\ \mathcal{F}_{\sigma\sigma'}(\mathbf{k}_1, \mathbf{k}_2, \tau) &\equiv \langle T_\tau c_{\mathbf{k}_1, \sigma}(\tau) c_{-\mathbf{k}_2, \sigma'}(0) \rangle,\end{aligned}\quad (10)$$

where $c_{\mathbf{k}, \sigma}$ is the annihilation operator for a *plane wave* state. In the presence of a scattering surface, these correlation functions will not be diagonal in momentum space.

Due to translational invariance in the y - and z -direction, it is natural to introduce the 4x4 Green's function in spin \times particle-hole space in a mixed representation, $\tilde{\mathbb{G}}(x_1, x_2, \mathbf{k}_\parallel; i\omega_n)$. We have defined $\mathbf{k}_\parallel = k_y \hat{\mathbf{y}} + k_z \hat{\mathbf{z}}$. The normal and anomalous components are $\tilde{\mathcal{G}}_{\sigma\sigma'}(x_1, x_2, \mathbf{k}_\parallel, \tau) = -\langle T_\tau c_{x_1, \mathbf{k}_\parallel, \sigma}(\tau) c_{x_2, \mathbf{k}_\parallel, \sigma'}^\dagger(0) \rangle$ and $\tilde{\mathcal{F}}_{\sigma\sigma'}(x_1, x_2, \mathbf{k}_\parallel, \tau) = \langle T_\tau c_{x_1, \mathbf{k}_\parallel, \sigma}(\tau) c_{x_2, -\mathbf{k}_\parallel, \sigma'}(0) \rangle$, respectively. The Green's function is determined by the Gor'kov equations (A3), which are presented in appendix A. The boundary conditions are

$$\tilde{\mathbb{G}}(x_1, x_2, \mathbf{k}_\parallel, i\omega_n) = 0, \quad x_1 = 0 \text{ or } x_2 = 0.\quad (11)$$

The pair potential in this mixed basis, $\Delta(x_1, x_2, \mathbf{k}_\parallel)$, should be determined self-consistently. Even though it may deviate significantly from the bulk near surfaces,^{21,22} we will approximate it by its bulk value. This approximation is expected to give qualitatively correct results.^{17,20} In appendix A it is shown that this approximation enables us to express the half-space Green's function in terms of bulk Green's functions. This may be realized by treating the surface as a wall of nonmagnetic impurities of infinite strength.³² The momentum space Green's function then becomes

$$\mathbb{G}(\mathbf{k}_1, \mathbf{k}_2, i\omega_n) = \left[\mathbb{G}_b(\mathbf{k}_1, i\omega_n) \delta(k_{1,x} - k_{2,x}) - \mathbb{G}_b(\mathbf{k}_1, i\omega_n) \tilde{\mathbb{G}}_b^{-1}(0, 0, \mathbf{k}_\parallel, i\omega_n) \mathbb{G}_b(\mathbf{k}_2, i\omega_n) \right] \delta(\mathbf{k}_{1,\parallel} - \mathbf{k}_{2,\parallel}).\quad (12)$$

To determine this, we need the inverse of the matrix

$$\tilde{\mathbb{G}}_b(0, 0, \mathbf{k}_\parallel, i\omega_n) = \int_{-\infty}^{\infty} dk_x \mathbb{G}_b(\mathbf{k}, i\omega_n).\quad (13)$$

Let us now define $\mathbf{k} \equiv (k_x, \mathbf{k}_\parallel)$ and $\bar{\mathbf{k}} \equiv (-k_x, \mathbf{k}_\parallel)$. From the previous subsection, we saw that the gaps $\chi_{\pm, \mathbf{k}}$ where unchanged upon reversal of the momentum. At this point we restrict ourselves to surfaces such that the

gaps are unchanged also when reversing the component of the momentum perpendicular to the surface only, *i.e.* $\chi_{\lambda, \bar{\mathbf{k}}} = \chi_{\lambda, \mathbf{k}}$. Although this is not a necessary requirement to determine the Green's function, it will simplify the calculations and be sufficient for the scenarios considered here. We will also assume $\xi_{\lambda, \bar{\mathbf{k}}} = \xi_{\lambda, \mathbf{k}}$. Using these approximations, the properties $G_\lambda(\bar{\mathbf{k}}, i\omega_n) = G_\lambda(\mathbf{k}, i\omega_n)$ and $F_\lambda(\bar{\mathbf{k}}, i\omega_n) = F_\lambda(\mathbf{k}, i\omega_n)$ follow from equations (8).

We now convert the k_x -integral in (13) to an energy integral. The integrand will be strongly peaked about the Fermi level. Thus, we apply the quasiclassical approximation of replacing all momentum-dependent quantities by their value at the Fermi level.³³ We introduce the notation

$$\mathbf{k}_F \equiv (k_{F,x}, \mathbf{k}_{\parallel}), \quad \bar{\mathbf{k}}_F \equiv (-k_{F,x}, \mathbf{k}_{\parallel}), \quad (14)$$

where $k_{F,x} \geq 0$ is determined by $\xi_{\mathbf{k}_F} = 0$ given \mathbf{k}_{\parallel} . We define the quasiclassical or ξ -integrated Green's functions by

$$\begin{aligned} g_{\lambda}(\mathbf{k}_F, i\omega_n) &= -\frac{i\omega_n}{\sqrt{\omega_n^2 + |\chi_{\lambda, \mathbf{k}_F}|^2}}, \\ f_{\lambda}(\mathbf{k}_F, i\omega_n) &= \frac{\chi_{\lambda, \mathbf{k}_F}}{\sqrt{\omega_n^2 + |\chi_{\lambda, \mathbf{k}_F}|^2}}. \end{aligned} \quad (15)$$

The integral over the normal Green's function in matrix (13) is found using

$$\frac{1}{2} \int_{-\infty}^{\infty} dk_x \sigma_{\hat{\mathbf{B}}_{\mathbf{k}}}^{\lambda} G_{\lambda}(\mathbf{k}, i\omega_n) = \pi N_{\lambda, \mathbf{k}_F}^x \sigma_{\hat{\mathbf{b}}_{\mathbf{k}_{\parallel}}}^{\lambda} g_{\lambda}(\mathbf{k}_F, i\omega_n), \quad (16)$$

where $N_{\lambda, \mathbf{k}_F}^x$ is $|\partial_{k_x} \xi_{\lambda, \mathbf{k}}|^{-1}$ taken at \mathbf{k}_F . The vector

$$\mathbf{b}_{\mathbf{k}_{\parallel}} = \frac{1}{2}(\hat{\mathbf{B}}_{\mathbf{k}_F} + \hat{\mathbf{B}}_{\bar{\mathbf{k}}_F}) \quad (17)$$

has the property $\mathbf{b}_{-\mathbf{k}_{\parallel}} = -\mathbf{b}_{\mathbf{k}_{\parallel}}$, but is not a unit vector. Similarly, the integral over the anomalous Green's function is obtained from

$$\frac{1}{2} \int_{-\infty}^{\infty} dk_x \sigma_{\hat{\mathbf{B}}_{\mathbf{k}}}^{\lambda} F_{\lambda}(\mathbf{k}, i\omega_n) = \pi N_{\lambda, \mathbf{k}_F}^x \sigma_{\hat{\mathbf{b}}_{\mathbf{k}_{\parallel}}}^{\lambda} f_{\lambda}(\mathbf{k}_F, i\omega_n). \quad (18)$$

We now assume that the difference in the density of states of the two spin-orbit split bands is small and may be neglected. Consequently, we also let $N_{+, \mathbf{k}_F}^x = N_{-, \mathbf{k}_F}^x \equiv N_{\mathbf{k}_F}^x$.⁴¹ This is not a necessary step in order to proceed, but it simplifies the calculations.

The inverse of the matrix (13) is then

$$\tilde{\mathbf{G}}_{\mathbf{b}}^{-1}(0, 0, \mathbf{k}_{\parallel}, i\omega_n) = \frac{1}{\pi K(\mathbf{k}_F, i\omega_n) N_{\mathbf{k}_F}^x} \sum_{\rho=\pm} \begin{pmatrix} \sigma_{\hat{\mathbf{b}}_{\mathbf{k}_{\parallel}}}^{\rho} g_{\rho}^*(\mathbf{k}_F, i\omega_n) & i\sigma_{\hat{\mathbf{b}}_{\mathbf{k}_{\parallel}}}^{\rho} \sigma_y f_{\rho}(\mathbf{k}_F, i\omega_n) \\ -i\sigma_y \sigma_{\hat{\mathbf{b}}_{\mathbf{k}_{\parallel}}}^{\rho} f_{\rho}^*(\mathbf{k}_F, i\omega_n) & -\sigma_y \sigma_{\hat{\mathbf{b}}_{\mathbf{k}_{\parallel}}}^{\rho} \sigma_y g_{\rho}(\mathbf{k}_F, i\omega_n) \end{pmatrix}. \quad (19)$$

We have introduced the function

$$K(\mathbf{k}_F, i\omega_n) = 2 \left[b_{+, \mathbf{k}_{\parallel}} + b_{-, \mathbf{k}_{\parallel}} \frac{\omega_n^2 + \text{Re}(\chi_{+, \mathbf{k}_F} \chi_{-, \mathbf{k}_F}^*)}{\sqrt{\omega_n^2 + |\chi_{+, \mathbf{k}_F}|^2} \sqrt{\omega_n^2 + |\chi_{-, \mathbf{k}_F}|^2}} \right], \quad (20)$$

where $b_{\pm, \mathbf{k}_{\parallel}} = 1 \pm |\mathbf{b}_{\mathbf{k}_{\parallel}}|^2$. Later, it will be apparent that zeros in $K(\mathbf{k}_F, i\omega_n)$ will correspond to surface bound states.

Introduce the simplified notation $G_{\lambda, 1} \equiv G_{\lambda}(\mathbf{k}_1, i\omega_n)$, $F_{\mu, 2} \equiv F_{\mu}(\mathbf{k}_2, i\omega_n)$ and $g_{\rho} \equiv g_{\rho}(\mathbf{k}_F, i\omega_n)$. No momentum index is needed on the latter since it depends only on the parallel momentum and $\mathbf{k}_{1, \parallel} = \mathbf{k}_{2, \parallel} \equiv \mathbf{k}_{\parallel}$. We are then ready to write down the half-space Green's function. The normal and anomalous parts, defined in (10), are

$$\begin{aligned} \mathcal{G}(\mathbf{k}_1, \mathbf{k}_2, i\omega_n) &= \frac{1}{2} \left\{ \sum_{\lambda} \sigma_{\hat{\mathbf{B}}_{\mathbf{k}}}^{\lambda} G_{\lambda, 1} \delta(k_{1,x} - k_{2,x}) \right. \\ &\quad \left. - \frac{1}{2\pi K(\mathbf{k}_F, i\omega_n) N_{\mathbf{k}_F}^x} \sum_{\lambda \rho \mu} \tilde{\sigma}_{\mathbf{k}_1, \mathbf{k}_2}^{\lambda \rho \mu} \left[G_{\lambda, 1} (g_{\rho}^* G_{\mu, 2} + f_{\rho} F_{\mu, 2}^*) + F_{\lambda, 1} (f_{\rho}^* G_{\mu, 2} - g_{\rho} F_{\mu, 2}^*) \right] \right\} \delta(\mathbf{k}_{1, \parallel} - \mathbf{k}_{2, \parallel}) \end{aligned} \quad (21)$$

and

$$\begin{aligned} \mathcal{F}(\mathbf{k}_1, \mathbf{k}_2, i\omega_n) &= -\frac{i}{2} \left\{ \sum_{\lambda} \sigma_{\hat{\mathbf{B}}_{\mathbf{k}}}^{\lambda} \sigma_y F_{\lambda, 1} \delta(k_{1,x} - k_{2,x}) \right. \\ &\quad \left. - \frac{1}{2\pi K(\mathbf{k}_F, i\omega_n) N_{\mathbf{k}_F}^x} \sum_{\lambda \rho \mu} \tilde{\sigma}_{\mathbf{k}_1, \mathbf{k}_2}^{\lambda \rho \mu} \sigma_y \left[G_{\lambda, 1} (g_{\rho}^* F_{\mu, 2} - f_{\rho} G_{\mu, 2}^*) + F_{\lambda, 1} (f_{\rho}^* F_{\mu, 2} + g_{\rho} G_{\mu, 2}^*) \right] \right\} \delta(\mathbf{k}_{1, \parallel} - \mathbf{k}_{2, \parallel}), \end{aligned} \quad (22)$$

respectively. These functions are found by inserting

equations (6) and (19) into equation (12).

We have defined the matrix

$$\tilde{\sigma}_{\mathbf{k}_1, \mathbf{k}_2}^{\lambda\rho\mu} = \sigma_{\hat{\mathbf{B}}_{\mathbf{k}_1}}^\lambda \sigma_{\mathbf{b}_{\mathbf{k}_2}}^\rho \sigma_{\hat{\mathbf{B}}_{\mathbf{k}_2}}^\mu \equiv \beta_{\mathbf{k}_1, \mathbf{k}_2}^{\lambda\rho\mu} \mathbb{1} + \boldsymbol{\alpha}_{\mathbf{k}_1, \mathbf{k}_2}^{\lambda\rho\mu} \cdot \boldsymbol{\sigma}, \quad (23)$$

where the expressions for the scalar $\beta_{\mathbf{k}_1, \mathbf{k}_2}^{\lambda\rho\mu}$ and the vector $\boldsymbol{\alpha}_{\mathbf{k}_1, \mathbf{k}_2}^{\lambda\rho\mu}$ are given in appendix B.

III. CALCULATION OF TUNNELING CURRENTS

Let us now consider a planar tunnel junction between two superconductors with spin-orbit split bands. We name the systems A and B and let the x -axis point perpendicular to the junction. In addition, we use the letter c for operators and \mathbf{k} for momenta on side A, and d and \mathbf{p} for the corresponding quantities on side B. The spin-orbit coupling is described by the vectors $\mathbf{B}_{\mathbf{k}}^A$ and $\mathbf{B}_{\mathbf{p}}^B$ on each side. These vectors are not necessarily equal. Let us briefly exemplify this by considering the Rashba spin-orbit coupling, $\mathbf{B}_{\mathbf{k}} = \alpha(\hat{\mathbf{n}} \times \mathbf{k})$, even though we will work with a general $\mathbf{B}_{\mathbf{k}}$. Here, the vector $\hat{\mathbf{n}}$ describes the direction of broken inversion symmetry of the crystal. This means that if the crystallographic orientation on side B is different from side A, $\mathbf{B}_{\mathbf{k}}^A$ and $\mathbf{B}_{\mathbf{p}}^B$ will point in different directions even when $\mathbf{k} = \mathbf{p}$.

The tunneling process is described by

$$H_T = \sum_{\sigma\sigma'} \int d\mathbf{k}d\mathbf{p} \left(\mathcal{T}_{\mathbf{k}\mathbf{p}, \sigma\sigma'} c_{\mathbf{k}\sigma}^\dagger d_{\mathbf{p}\sigma'} + \mathcal{T}_{\mathbf{k}\mathbf{p}, \sigma\sigma'}^* d_{\mathbf{p}\sigma'}^\dagger c_{\mathbf{k}\sigma} \right). \quad (24)$$

The validity of results using perturbation theory in the tunneling Hamiltonian formalism has been showed by Prange.³⁴

We emphasize that the systems are described in terms of *plane wave* states. Thus, $\mathcal{T}_{\mathbf{k}\mathbf{p}, \sigma\sigma'}$ is the transfer amplitude from an incoming plane wave state with momentum \mathbf{p} on side B to an outgoing plane wave state with momentum \mathbf{k} on side A. When scattering a plane wave on a barrier, the perpendicular momentum of the transmitted wave points in the same direction as the incoming wave. In addition, we assume that the tunneling process conserves spin. These properties result in

$$\mathcal{T}_{\mathbf{k}\mathbf{p}, \sigma\sigma'} \equiv T_{\mathbf{k}, \mathbf{p}} \Theta[k_x p_x] \delta_{\sigma, \sigma'}, \quad (25)$$

where $\Theta[x]$ is the Heaviside step function. Time-reversal symmetry also demands $T_{-\mathbf{k}, -\mathbf{p}}^* = T_{\mathbf{k}, \mathbf{p}}$.

Of course, there is also an amplitude for the incoming plane wave being reflected. However, when treating equation (24) as a perturbation, the current will be expressed as Green's functions of the unperturbed systems A and B. Thus, the reflection is taken into account by using the half-space Green's functions obtained in the previous section.

The current from side B to side A is defined as $I(t) = -e\langle \dot{\mathcal{N}}_A \rangle$, where \mathcal{N}_A is the total charge operator on side A and the operator $\dot{\mathcal{N}}_A$ is given by the Heisenberg equation

$\dot{\mathcal{N}}_A = i[H_T, \mathcal{N}_A]$. Treating the tunneling Hamiltonian as a perturbation, the Kubo formula gives $I(t) = I_{\text{qp}} + I_J(t)$,³⁵ where

$$\begin{aligned} I_{\text{qp}} &= -2e \text{Im} \Phi(eV), \\ I_J(t) &= 2e \text{Im} \left[e^{-2ieVt} \Psi(eV) \right]. \end{aligned} \quad (26)$$

In the imaginary time formalism, when defining $M(\tau) \equiv \sum_{\sigma\sigma'} \int d\mathbf{k}d\mathbf{p} c_{\mathbf{k}\sigma}^\dagger(\tau) d_{\mathbf{p}\sigma'}(\tau)$, we have

$$\begin{aligned} \Phi(i\omega_\nu) &= - \int_0^\beta d\tau e^{i\omega_\nu \tau} \langle T_\tau M(\tau) M^\dagger(0) \rangle, \\ \Psi(i\omega_\nu) &= - \int_0^\beta d\tau e^{i\omega_\nu \tau} \langle T_\tau M(\tau) M(0) \rangle. \end{aligned} \quad (27)$$

The time dependence of the operators are given by the unperturbed Hamiltonian and the expectation values are to be taken in the unperturbed state. The voltage is defined by $eV = \mu_A - \mu_B$. The bosonic Matsubara frequency is $\omega_\nu = 2\nu\pi/\beta$, which will be subject to $i\omega_\nu \rightarrow eV + i0^+$.

Equations (27) may be written as

$$\begin{aligned} \Phi(i\omega_\nu) &= \frac{1}{\beta} \int d\mathbf{k}_1 d\mathbf{k}_2 d\mathbf{p}_1 d\mathbf{p}_2 T_{\mathbf{k}_1, \mathbf{p}_1} T_{\mathbf{k}_2, \mathbf{p}_2}^* \\ &\times \sum_{\omega_n} \text{Tr} \left[\mathcal{G}_A(\mathbf{k}_2, \mathbf{k}_1, i\omega_n - i\omega_\nu) \mathcal{G}_B(\mathbf{p}_1, \mathbf{p}_2, i\omega_n) \right] \end{aligned} \quad (28)$$

and

$$\begin{aligned} \Psi(i\omega_\nu) &= \frac{1}{\beta} \int d\mathbf{k}_1 d\mathbf{k}_2 d\mathbf{p}_1 d\mathbf{p}_2 T_{\mathbf{k}_1, \mathbf{p}_1} T_{\mathbf{k}_2, \mathbf{p}_2}^* \\ &\times \sum_{\omega_n} \text{Tr} \left[\mathcal{F}_A^\dagger(\mathbf{k}_2, \mathbf{k}_1, i\omega_n - i\omega_\nu) \mathcal{F}_B(\mathbf{p}_1, \mathbf{p}_2, i\omega_n) \right], \end{aligned} \quad (29)$$

where the components of the Green's functions are defined in (10) and Tr denotes a trace in spin space.

As before, when converting the momentum integrals to energy integrals, we replace all momentum-dependent quantities by their value on the Fermi level. The density of states $N(\mathbf{k}_F)$ at the Fermi level is assumed equal in both bands. In addition, we assume $N(\bar{\mathbf{k}}_F) = N(\mathbf{k}_F)$ and $T_{\bar{\mathbf{k}}_F, \bar{\mathbf{p}}_F} = T_{\mathbf{k}_F, \mathbf{p}_F}$.

A. The quasiparticle current

Inserting the Green's function (21) in equation (28), one arrives at

$$\begin{aligned} \Phi(i\omega_\nu) &= \frac{\pi^2}{4} \int' d\mathbf{k} \int' d\mathbf{p} |T_{\mathbf{k}_F, \mathbf{p}_F}|^2 N^A(\mathbf{k}_F) N^B(\mathbf{p}_F) \\ &\times \left\{ A_1^{\lambda\gamma}(\mathbf{k}_F, \mathbf{p}_F) S_1^{\lambda\gamma}(\mathbf{k}_F, \mathbf{p}_F, i\omega_\nu) \right. \\ &\quad - \frac{1}{2} A_2^{\lambda\gamma\eta\nu}(\mathbf{k}_F, \mathbf{p}_F) S_2^{\lambda\gamma\eta\nu}(\mathbf{k}_F, \mathbf{p}_F, i\omega_\nu) \\ &\quad - \frac{1}{2} A_3^{\lambda\rho\mu\gamma}(\mathbf{k}_F, \mathbf{p}_F) S_3^{\lambda\rho\mu\gamma}(\mathbf{k}_F, \mathbf{p}_F, i\omega_\nu) \\ &\quad \left. + \frac{1}{4} A_4^{\lambda\rho\mu\gamma\eta\nu}(\mathbf{k}_F, \mathbf{p}_F) S_4^{\lambda\rho\mu\gamma\eta\nu}(\mathbf{k}_F, \mathbf{p}_F, i\omega_\nu) \right\}, \end{aligned} \quad (30)$$

where *repeated greek indices are to be summed over*. The prime indicates that the integrals over the Fermi surfaces are restricted to positive \hat{k}_x, \hat{p}_x . The A_i 's are defined by⁴²

$$\begin{aligned} A_1^{\lambda\gamma}(\mathbf{k}, \mathbf{p}) &= \text{Tr} \sigma_{\hat{\mathbf{B}}_k^A}^\lambda \sigma_{\hat{\mathbf{B}}_p^B}^\gamma + \text{Tr} \sigma_{\hat{\mathbf{B}}_k^B}^\lambda \sigma_{\hat{\mathbf{B}}_p^A}^\gamma, \\ A_2^{\lambda\gamma\eta\nu}(\mathbf{k}, \mathbf{p}) &= \text{Tr} \sigma_{\hat{\mathbf{B}}_k^A}^\lambda \tilde{\sigma}_{\mathbf{p}, \mathbf{p}}^{\gamma\eta\nu} + \text{Tr} \sigma_{\hat{\mathbf{B}}_k^B}^\lambda \tilde{\sigma}_{\tilde{\mathbf{p}}, \tilde{\mathbf{p}}}^{\gamma\eta\nu}, \\ A_3^{\lambda\rho\mu\gamma}(\mathbf{k}, \mathbf{p}) &= \text{Tr} \tilde{\sigma}_{\mathbf{k}, \mathbf{k}}^{\lambda\rho\mu} \sigma_{\hat{\mathbf{B}}_p^B}^\gamma + \text{Tr} \tilde{\sigma}_{\tilde{\mathbf{k}}, \tilde{\mathbf{k}}}^{\lambda\rho\mu} \sigma_{\hat{\mathbf{B}}_p^A}^\gamma, \\ A_4^{\lambda\rho\mu\gamma\eta\nu}(\mathbf{k}, \mathbf{p}) &= \text{Tr} \tilde{\sigma}_{\mathbf{k}, \mathbf{k}}^{\lambda\rho\mu} \tilde{\sigma}_{\mathbf{p}, \mathbf{p}}^{\gamma\eta\nu} + \text{Tr} \tilde{\sigma}_{\tilde{\mathbf{k}}, \tilde{\mathbf{k}}}^{\lambda\rho\mu} \tilde{\sigma}_{\tilde{\mathbf{p}}, \tilde{\mathbf{p}}}^{\gamma\eta\nu} \\ &\quad + \text{Tr} \tilde{\sigma}_{\mathbf{k}, \mathbf{k}}^{\lambda\rho\mu} \tilde{\sigma}_{\tilde{\mathbf{p}}, \tilde{\mathbf{p}}}^{\gamma\eta\nu} + \text{Tr} \tilde{\sigma}_{\tilde{\mathbf{k}}, \tilde{\mathbf{k}}}^{\lambda\rho\mu} \tilde{\sigma}_{\mathbf{p}, \mathbf{p}}^{\gamma\eta\nu}. \end{aligned} \quad (31)$$

These quantities depend on $\hat{\mathbf{B}}_k^A, \hat{\mathbf{B}}_k^B, \hat{\mathbf{B}}_p^A, \hat{\mathbf{B}}_p^B$ and explicit expressions are given in appendix B. The S_i 's depend on the momenta through the gaps and are defined as

$$\begin{aligned} S_1^{\lambda\gamma}(\mathbf{k}, \mathbf{p}, i\omega_\nu) &= \frac{1}{\beta} \sum_{\omega_n} g_\lambda^A(\mathbf{k}, i\omega_n - i\omega_\nu) g_\gamma^B(\mathbf{p}, i\omega_n), \\ S_2^{\lambda\gamma\eta\nu}(\mathbf{k}, \mathbf{p}, i\omega_\nu) &= \frac{1}{\beta} \sum_{\omega_n} g_\lambda^A(\mathbf{k}, i\omega_n - i\omega_\nu) \Gamma_{\gamma\eta\nu}^B(\mathbf{p}, i\omega_n), \\ S_3^{\lambda\rho\mu\gamma}(\mathbf{k}, \mathbf{p}, i\omega_\nu) &= \frac{1}{\beta} \sum_{\omega_n} \Gamma_{\lambda\rho\mu}^A(\mathbf{k}, i\omega_n - i\omega_\nu) g_\gamma^B(\mathbf{p}, i\omega_n), \\ S_4^{\lambda\rho\mu\gamma\eta\nu}(\mathbf{k}, \mathbf{p}, i\omega_\nu) &= \frac{1}{\beta} \sum_{\omega_n} \Gamma_{\lambda\rho\mu}^A(\mathbf{k}, i\omega_n - i\omega_\nu) \Gamma_{\gamma\eta\nu}^B(\mathbf{p}, i\omega_n). \end{aligned} \quad (32)$$

The function $g_\lambda(\mathbf{k}, i\omega_n)$ was defined in equation (15). The function $\Gamma_{\lambda\rho\mu}(\mathbf{k}, i\omega_n)$ is

$$\Gamma_{\lambda\rho\mu}(\mathbf{k}, i\omega_n) = \frac{g_\lambda [g_\rho^* g_\mu + f_\rho f_\mu^*] + f_\lambda [f_\rho^* g_\mu - g_\rho f_\mu^*]}{K(\mathbf{k}, i\omega_n)}, \quad (33)$$

where the arguments of the g 's and f 's were omitted for clarity. Note that $\Gamma_{\lambda\rho\mu}(\mathbf{k}_F, i\omega_n)$ does not depend on $N_{\mathbf{k}_F}^x$.

In equation (30), we have reached the point at which the current I_{qp} is expressed as two surface integrals over half of the Fermi surface on each side. In addition, one is left with the Matsubara sums which may be converted to energy integrals. To get further, one must insert the appropriate angular dependence of the quantities $\chi_{\lambda, \mathbf{k}_F}$, $\hat{\mathbf{B}}_{\mathbf{k}_F}$, $N(\mathbf{k}_F)$ on each side as well as $|T_{\mathbf{k}_F, \mathbf{p}_F}|$. In most cases, the remaining integrals need to be performed numerically. Both the energy and angle integrands contain integrable singularities which must be handled with care.

We will now assume that the two gaps $\chi_{\pm, \mathbf{k}}$ are phase-locked due to the internal Josephson coupling. We write out the phase explicitly, such that $\chi_{\pm, \mathbf{k}}^A \rightarrow \chi_{\pm, \mathbf{k}}^A e^{i\theta^A}$. $\chi_{+, \mathbf{k}}^A$ and $\chi_{-, \mathbf{k}}^A$ are real from now on, but not necessarily of the same sign. Obviously, the same also applies to the gaps on side B.

To obtain the current I_{qp} , we need $\text{Im} \Phi(i\omega_\nu)$. Since the A_i 's are real (see appendix B), the only complex parts are contained in the Matsubara sums. By converting the sums to contour integrals in the complex plane and deforming the contour, one finds that $\text{Im} S_i(eV + i0^+)$ may be expressed as energy integrals containing the functions $\text{Im} g_\lambda(\mathbf{k}, E + i0^+)$, $\text{Im} \Gamma_{\lambda\rho\mu}(\mathbf{k}, E + i0^+)$ and the Fermi-Dirac distribution $n_F(E)$. Details of this procedure and the choice of appropriate branch cuts are found in appendix C. The first function is proportional to the usual bulk density of states

$$\text{Im} g_\lambda(\mathbf{k}, E + i0^+) = -\Theta[|E| - |\chi_{\lambda, \mathbf{k}}|] \frac{|E|}{\sqrt{E^2 - |\chi_{\lambda, \mathbf{k}}|^2}} \quad (34)$$

As before, $\Theta[x]$ is the Heaviside step function. The second function is somewhat complicated, but may be written as

$$\text{Im} \Gamma_{\lambda\rho\mu}(\mathbf{k}, E + i0^+) = \Theta[|E| - |\chi_{m, \mathbf{k}}|] P_{\lambda\rho\mu}(E) + \Theta[|\chi_{m, \mathbf{k}}| - |E|] \Theta[-\chi_{+, \mathbf{k}} \chi_{-, \mathbf{k}}] \bar{P}_{\lambda\rho\mu}(E) \delta(|E| - E_{0, \mathbf{k}}), \quad (35)$$

where $|\chi_{m, \mathbf{k}}| \equiv \min(|\chi_{+, \mathbf{k}}|, |\chi_{-, \mathbf{k}}|)$. The functions $P_{\lambda\rho\mu}(E)$ and $\bar{P}_{\lambda\rho\mu}(E)$ are even functions of E and may be found by using equations (C2) and (C3) in appendix C. If one interprets $\text{Im} \Gamma_{\lambda\rho\mu}(\mathbf{k}, E + i0^+)$ as a density of states, the first term describes a continuum above the smallest gap. However, the second term describes *additional discrete states below the smallest gap*. These are the Andreev bound states induced by the reflection from the surface. Note that

they appear only when the sign of the two gaps differ, as was also noted in Ref. 20. The energy $E_{0,\hat{\mathbf{k}}}$ is the positive solution to the equation

$$b_{-, \mathbf{k}_{\parallel}} \left(\chi_{+, \mathbf{k}} \chi_{-, \mathbf{k}} - E_{0, \hat{\mathbf{k}}}^2 \right) + b_{+, \mathbf{k}_{\parallel}} \sqrt{|\chi_{+, \mathbf{k}}|^2 - E_{0, \hat{\mathbf{k}}}^2} \sqrt{|\chi_{-, \mathbf{k}}|^2 - E_{0, \hat{\mathbf{k}}}^2} = 0 \quad (36)$$

and is measured relative to the Fermi level. Thus, we get a band of low energy surface bound states in the part of momentum space where $\chi_{+, \mathbf{k}} \chi_{-, \mathbf{k}} < 0$. Equation (36) corresponds to equation (14) of Ref. 20, but here we have made no assumption of the particular form of $\mathbf{B}_{\mathbf{k}}$.

Let us also comment on what happens in the limit of a singlet superconductor. From equation (5), we see that this limit corresponds to $\chi_{+, \mathbf{k}} = \chi_{-, \mathbf{k}}$. In that case, there are obviously no Andreev bound states and $\Gamma_{\lambda\rho\mu}(\mathbf{k}, i\omega_n) = g_+(\mathbf{k}, i\omega_n)/4 = g_-(\mathbf{k}, i\omega_n)/4$. The current I_{qp} then equals the result obtained using bulk Green's function.^{35,36}

Whereas the limit $\chi_{+, \mathbf{k}} = \chi_{-, \mathbf{k}}$ corresponds to a singlet superconductor, setting the gaps to zero corresponds to a normal metal. The current will in those cases not depend on the nature of the spin-orbit coupling vector $\mathbf{B}_{\mathbf{k}}$. The reader may wonder why there are no remnants of the spin-orbit coupling in these limits. This is a consequence of the approximation of equal densities of states for the two bands.

B. The Josephson current

The two-particle current is found by inserting the Green's function (22) in equation (29), giving

$$\begin{aligned} \Psi(i\omega_\nu) = & \frac{\pi^2}{4} \int' d\hat{\mathbf{k}} \int' d\hat{\mathbf{p}} |T_{\mathbf{k}_F, \mathbf{p}_F}|^2 N^A(\mathbf{k}_F) N^B(\mathbf{p}_F) \\ & \times \left\{ A_1^{\lambda\gamma}(\mathbf{k}_F, \mathbf{p}_F) \tilde{S}_1^{\lambda\gamma}(\mathbf{k}_F, \mathbf{p}_F, i\omega_\nu) \right. \\ & - \frac{1}{2} A_2^{\lambda\gamma\eta\nu}(\mathbf{k}_F, \mathbf{p}_F) \tilde{S}_2^{\lambda\gamma\eta\nu}(\mathbf{k}_F, \mathbf{p}_F, i\omega_\nu) \\ & - \frac{1}{2} A_3^{\lambda\rho\mu\gamma}(\mathbf{k}_F, \mathbf{p}_F) \tilde{S}_3^{\lambda\rho\mu\gamma}(\mathbf{k}_F, \mathbf{p}_F, i\omega_\nu) \\ & \left. + \frac{1}{4} A_4^{\lambda\rho\mu\gamma\eta\nu}(\mathbf{k}_F, \mathbf{p}_F) \tilde{S}_4^{\lambda\rho\mu\gamma\eta\nu}(\mathbf{k}_F, \mathbf{p}_F, i\omega_\nu) \right\}. \end{aligned} \quad (37)$$

As before, the integrals are restricted to positive \hat{k}_x, \hat{p}_x and repeated greek indices are summed over. The \tilde{S}_i 's

are defined as

$$\begin{aligned} \tilde{S}_1^{\lambda\gamma}(\mathbf{k}, \mathbf{p}, i\omega_\nu) &= \frac{1}{\beta} \sum_{\omega_n} f_\lambda^{*A}(\mathbf{k}, i\omega_n - i\omega_\nu) f_\gamma^B(\mathbf{p}, i\omega_n), \\ \tilde{S}_2^{\lambda\gamma\eta\nu}(\mathbf{k}, \mathbf{p}, i\omega_\nu) &= \frac{1}{\beta} \sum_{\omega_n} f_\lambda^{*A}(\mathbf{k}, i\omega_n - i\omega_\nu) \Lambda_{\gamma\eta\nu}^B(\mathbf{p}, i\omega_n), \\ \tilde{S}_3^{\lambda\rho\mu\gamma}(\mathbf{k}, \mathbf{p}, i\omega_\nu) &= \frac{1}{\beta} \sum_{\omega_n} \Lambda_{\lambda\rho\mu}^{*A}(\mathbf{k}, i\omega_n - i\omega_\nu) f_\gamma^B(\mathbf{p}, i\omega_n), \\ \tilde{S}_4^{\lambda\rho\mu\gamma\eta\nu}(\mathbf{k}, \mathbf{p}, i\omega_\nu) &= \frac{1}{\beta} \sum_{\omega_n} \Lambda_{\lambda\rho\mu}^{*A}(\mathbf{k}, i\omega_n - i\omega_\nu) \Lambda_{\gamma\eta\nu}^B(\mathbf{p}, i\omega_n). \end{aligned} \quad (38)$$

The function $f_\lambda(\mathbf{k}, i\omega_n)$ is defined in (15) and $\Lambda_{\lambda\rho\mu}(\mathbf{k}, i\omega_n)$ is

$$\Lambda_{\lambda\rho\mu}(\mathbf{k}, i\omega_n) = \frac{g_\lambda(g_\rho^* f_\mu - f_\rho g_\mu^*) + f_\lambda(f_\rho^* f_\mu + g_\rho g_\mu^*)}{K(\mathbf{k}, i\omega_n)}. \quad (39)$$

As in the previous subsection, we assume that the gaps are phase-locked, *i.e.* $\chi_{\pm, \mathbf{k}}^A \rightarrow \chi_{\pm, \mathbf{k}}^A e^{i\theta^A}$ and treat $\chi_{\pm, \mathbf{k}}^{A(B)}$ as real.

In the limit of a singlet superconductor, $\Lambda_{\lambda\rho\mu}(\mathbf{k}, i\omega_n) = f_+(\mathbf{k}, i\omega_n)/4 = f_-(\mathbf{k}, i\omega_n)/4$. The Josephson current reduces to the result found using bulk Green's functions.³⁷

It should be noted that (37) is a tunneling limit expression. Thus, it may not capture all the unusual phenomena that arise when Andreev bound states contribute to Josephson currents.³⁸

IV. RESULTS

In this section, we consider a junction consisting of two equal superconductors and present numerical results on the quasiparticle and Josephson current. We choose to study the Rashba interaction

$$\mathbf{B}_{\mathbf{k}} = \alpha (\hat{\mathbf{n}} \times \mathbf{k}), \quad (40)$$

both because of its simplicity and its relevance to real materials like CePt₃Si (Ref. 27) and Cd₂Re₂O₇ (Ref. 29). The vector $\hat{\mathbf{n}}$ represents the direction of broken inversion symmetry of the crystal.

We restrict ourselves to junctions where $\hat{\mathbf{n}}^A$ and $\hat{\mathbf{n}}^B$ are perpendicular to the tunneling direction, *i.e.* $\hat{\mathbf{n}}^{A(B)} \cdot \hat{\mathbf{x}} = 0$. The angle ζ is defined by

$$\cos \zeta \equiv \hat{\mathbf{n}}^A \cdot \hat{\mathbf{n}}^B. \quad (41)$$

Of course, from an experimental point of view, only discrete values of the angle ζ may be realizable.

The variation of the current with ζ is a result of the facts that $\hat{\mathbf{n}}$ determines the spin structure of the spin-orbit split bands and that spin is conserved in the tunneling process. It should be noted that replacing one of the superconductors by a ferromagnet with magnetization \mathbf{M}^B and varying $\hat{\mathbf{n}}^A \cdot \mathbf{M}^B$ would not necessarily give similar conductance variations.⁴³

A. The quasiparticle current

We now present numerical results on the quasiparticle current I_{qp} given by equation (30). In addition to the choice of Rashba spin-orbit coupling, we also need the angular dependence of the gaps $\chi_{\pm, \mathbf{k}}$. As before, we write the phase explicitly, such that $\chi_{+, \mathbf{k}}$ and $\chi_{-, \mathbf{k}}$ are real.

We consider the same gaps as in Refs. 8 and 20, given by $\eta_{\mathbf{k}, S} = \Psi$ and $\eta_{\mathbf{k}, T} = \Delta |\hat{\mathbf{n}} \times \hat{\mathbf{k}}|$. The singlet and triplet components, $\eta_{\mathbf{k}, S}$ and $\eta_{\mathbf{k}, T}$, are defined in equations (4) and (5). Ψ and Δ are treated as constants for simplicity. We also assume that $\Psi \geq 0$ and $\Delta \geq 0$ without loss of generality. The gaps in the spin-orbit split bands are then

$$\chi_{\pm, \mathbf{k}} = \Psi \pm \Delta |\hat{\mathbf{n}} \times \hat{\mathbf{k}}|. \quad (42)$$

Let us define $q = \Psi/\Delta$. Whereas $\chi_{+, \mathbf{k}}$ is fully gapped if $q > 0$, the gap $\chi_{-, \mathbf{k}}$ contains line nodes if $0 < q < 1$. See Ref. 8 for details. At this point, we should mention that other explanations of line nodes in CePt₃Si have been put forward.^{7,9}

It is also for $q < 1$ that we may expect Andreev bound states at the surface, since $\chi_{+, \mathbf{k}} \chi_{-, \mathbf{k}} < 0$ on a part of the Fermi surface in that case. However, one should note that formation of Andreev bound states does not depend on the presence of gap nodes. Isotropic $\chi_{\pm, \mathbf{k}}$ with different signs will also result in subgap surface bound states.

For simplicity, we assume a spherical Fermi surface and let the density of states be constant over the Fermi surface, $N(\mathbf{k}_F) = N$. Let us introduce spherical coordinates by $\hat{\mathbf{k}} = (\cos \phi \sin \theta, \sin \phi \sin \theta, \cos \theta)$. As mentioned before, the x -axis is perpendicular to the junction. In addition, we let $\hat{\mathbf{n}}^A$ and $\hat{\mathbf{n}}^B$ point along or opposite to the $\hat{\mathbf{z}}$ -direction. The gaps are then given by $\chi_{\pm, \mathbf{k}}/\Delta = q \pm \sin \theta$. For $q < 1$, Andreev bound states are formed for momenta with $\arcsin(q) < \theta < \pi - \arcsin(q)$. As mentioned in section III A, these surface bound states form below the smallest gap, *i.e.* below $|\chi_{-, \mathbf{k}}|/\Delta = |q - \sin \theta|$. Figure 1 shows the spectrum of Andreev bound states $E_{0, \hat{\mathbf{k}}}$ in the case $q = 0$. The dependence on the azimuthal angle ϕ is shown for three different polar angles θ . We see that $E_{0, \hat{\mathbf{k}}} \rightarrow 0$ as $\phi \rightarrow 0$, which corresponds to $k_y = 0$ and thus $|\mathbf{b}_{\mathbf{k}_{\parallel}}| = 0$. The maximal value of $E_{0, \hat{\mathbf{k}}}$ is given by $|q - \sin \theta|$.

The tunneling matrix element, defined in equations (24) and (25), will typically favour momenta with a large

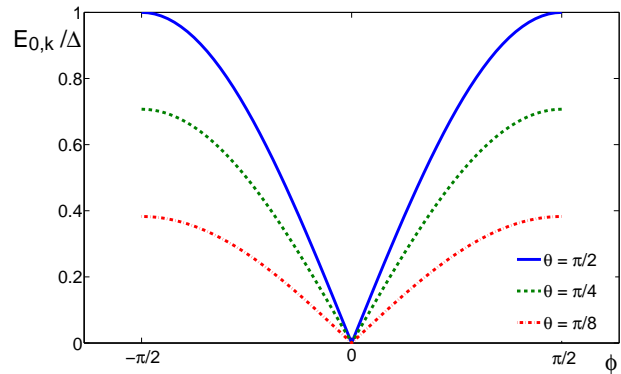


FIG. 1: (Color online) Energy spectrum for the bound states $E_{0, \hat{\mathbf{k}}}$ in the case $q = 0$. The dependence on the azimuthal angle ϕ is shown for three different polar angles θ .

component in the tunneling direction. Also, in the case of a smooth barrier, the parallel momentum is conserved in the tunneling process. Thus, we assume that

$$|T_{\mathbf{k}_F, \mathbf{p}_F}|^2 = t \hat{k}_x \hat{p}_x \delta(\hat{\mathbf{k}}_{\parallel} - \hat{\mathbf{p}}_{\parallel}) \quad (43)$$

will capture the qualitative features of the tunneling matrix element, where t is a constant.⁴⁴

One may show that the variation of the current with the angle ζ disappears when only perpendicular momenta contribute. In other words, the effect is dependent on a finite tunneling cone, where also nonzero parallel momenta contribute to the current.

Tunneling spectroscopy on superconductors are interesting at low temperatures. At higher temperatures, sharp features giving information on pairing states may be smeared out. Thus, we investigate the limit of zero temperature here. However, for $q < 1$, the current at low voltage is dominated by resonant transport between Andreev bound states. This is contained in the sum $S_4^{\lambda\rho\mu\gamma\nu}(\mathbf{k}_F, \mathbf{p}_F, i\omega_\nu)$, where a product of two delta distributions enters. At zero temperature, this leads to a discontinuity at $V = 0$, where the current jumps from zero to a finite value. The discontinuity disappears for nonzero temperatures and a sharp zero bias conductance peak appears. To get realistic current-voltage diagrams, we therefore retain a small temperature ($T/\Delta = 0.015$) in this particular term, such that this discontinuity at zero voltage is smeared out. Such a small temperature will have no significant effect on the other terms.

The current-voltage diagrams for several q are now presented, where we have defined $i_{\text{qp}} \equiv -I_{\text{qp}}/(2e\pi^2 t^2 N^2)$. We consider the cases of $\zeta = 0$ and $\zeta = \pi$, *i.e.* equal and opposite directions of broken inversion symmetry. In addition, we present the differential conductance $G(eV) \equiv d i_{\text{qp}}/d(eV)$, which may be directly accessible in experiments. The latter has been obtained through a Savitzky-Golay smoothing filter³⁹ to remove noise from the numerical integration.

We start by considering the $q = 0$ case, which corresponds to a pure spin triplet state. The gaps $\chi_{+,\mathbf{k}}$ and $\chi_{-,\mathbf{k}}$ are then of opposite signs on the entire Fermi surface except at $\hat{\mathbf{k}}_F = \pm\hat{\mathbf{n}}$, where they have point nodes. Figure 2 shows the current-voltage diagram when $q = 0$. The differential conductance is presented in figure 3. The large current at small voltages is due to transport between Andreev bound states on each side. This gives rise to a zero bias conductance peak followed by negative differential resistance. Similar phenomena appear in some d -wave junctions.³⁸ We observe that there is no difference between the cases $\zeta = 0$ and $\zeta = \pi$ in the pure triplet case. As stated before, this is also the case for the pure singlet case, $q \rightarrow \infty$.⁴⁵ However, we will see that this changes for finite q , when the gap is a mixture of singlet and triplet.

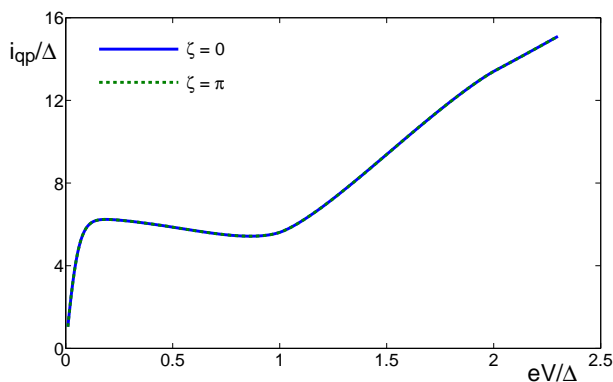


FIG. 2: (Color online) Current-voltage diagram in a Josephson junction when $q = \Psi/\Delta = 0$. Transport between Andreev bound states dominates for small voltages. There is no dependence on ζ in this pure triplet case.

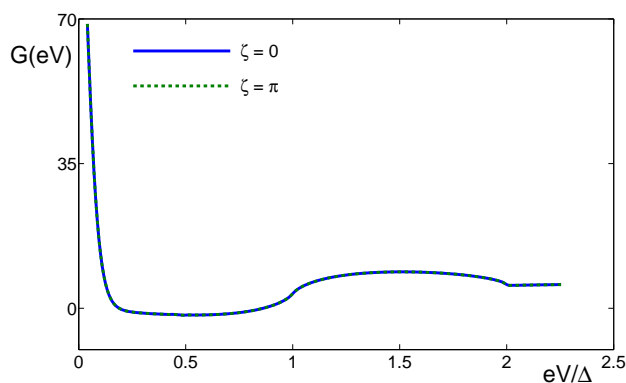


FIG. 3: (Color online) Differential conductance as a function of voltage when $q = 0$. For small voltages, the zero bias conductance peak followed by negative differential resistance is due to transport between Andreev bound states on each side. There is no dependence on ζ in this pure triplet case.

Figure 4 shows the current-voltage diagram in the case

$q = 0.4$. In this case, $\chi_{+,\mathbf{k}}$ is fully gapped (although anisotropic) whereas the gap $\chi_{-,\mathbf{k}}$ has got line nodes at $\theta \approx 23.6^\circ$ and $\theta \approx 66.4^\circ$. Andreev bound states exist between these angles. Observe that the cases $\zeta = 0$ and $\zeta = \pi$ differs. This becomes clearer when studying the differential conductance in figure 5. We do not attempt to explain every feature in this figure, as this depends on the particular pairing state chosen. In addition, some of these features might also be smeared out in experimental results. However, the important thing to notice, which might be observable, is the qualitative difference of a junction with equal $\hat{\mathbf{n}}$ -vectors ($\zeta = 0$) and one with opposite $\hat{\mathbf{n}}$ -vectors ($\zeta = \pi$).

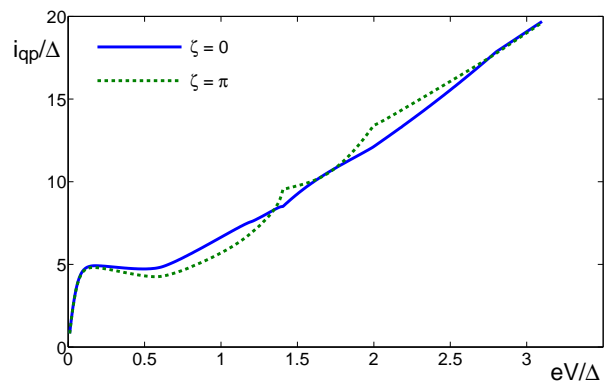


FIG. 4: (Color online) Current-voltage diagram when $q = 0.4$. Transport between Andreev bound states dominates for small voltages.

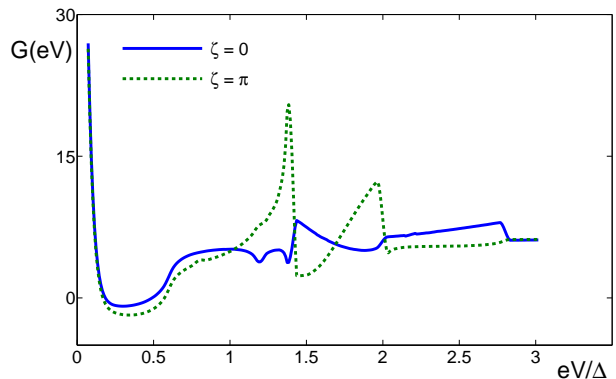


FIG. 5: (Color online) Differential conductance in the case $q = 0.4$. Transport between Andreev bound states dominates for small voltages.

The next current-voltage diagram, presented in figure 6, is for $q = 1$. Then, the line nodes have moved to the equator ($\theta = \pi/2$) and will disappear for $q > 1$. Now, there is no part of the Fermi surface where $\chi_{+,\mathbf{k}}\chi_{-,\mathbf{k}} < 0$, such that there are no Andreev bound states. In the differential conductance in figure 7, there is a clear difference between $\zeta = 0$ and $\zeta = \pi$. See Ref. 24 for a

simplified discussion of why this occurs.

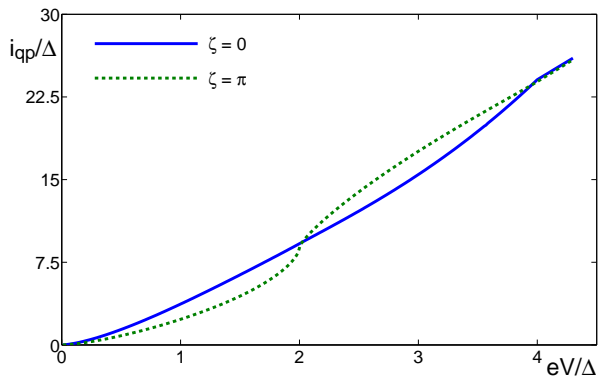


FIG. 6: (Color online) Current-voltage diagram when $q = 1$. At this point, there are no Andreev bound states.

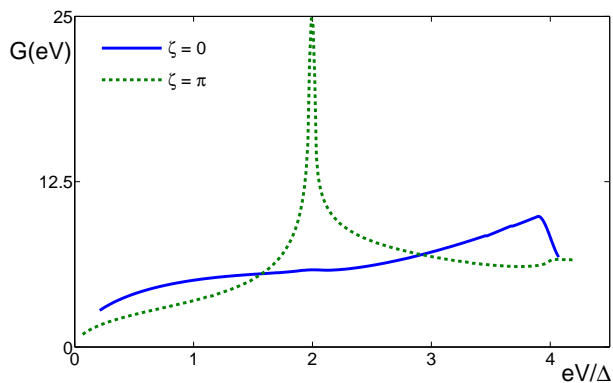


FIG. 7: (Color online) Differential conductance when $q = 1$. Note the qualitative difference in the two cases for $eV/\Delta < 4$.

Finally, we examine the scenario where the singlet to triplet ratio is $q = 2$. At this value, both $\chi_{+,\mathbf{k}}$ and $\chi_{-,\mathbf{k}}$ are fully gapped and of the same sign. The current-voltage diagram is given in figure 8 and the differential conductance in 9. Above $eV/\Delta = 2$, the behaviour is similar to the $q = 1$ case.

In the cases $q = 1$ and $q = 2$, we observe that the graphs differ in the region $2(q-1) < eV/\Delta < 2(q+1)$. This will also be the case for higher values of q , but the width of this region ($2(q+1) - 2(q-1) = 4$) becomes small relative to the voltages at which the graphs differ ($eV/\Delta \approx 2q$). In the limit $q \rightarrow \infty$, we are left with the singlet result, with a single step in the current for both $\zeta = 0$ and $\zeta = \pi$.

B. The Josephson current

We now move on to the Josephson current, given by equation (37). This has not been investigated in as much

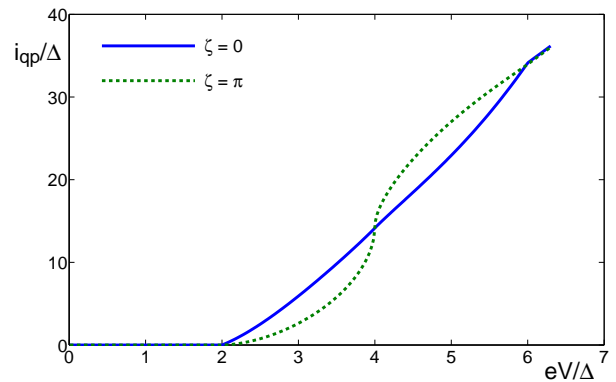


FIG. 8: (Color online) Current-voltage diagram when $q = 2$. At this point, both bands are fully gapped.

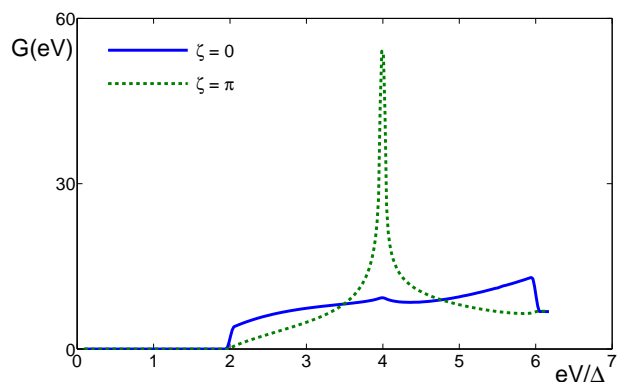


FIG. 9: (Color online) Differential conductance when $q = 2$. The two cases of $\zeta = 0$ and $\zeta = \pi$ differ significantly when $2 < eV/\Delta < 6$.

detail as the quasiparticle current. In this section, we only suggest that the critical Josephson junction at zero voltage may depend on the angle ζ between the axes of broken inversion symmetry of the crystal. We make no attempt to give any quantitative estimates here, since this depends not only on the particular pairing state of the material in question, but also on several other issues, like the details of the tunneling matrix elements. Only experiments can determine whether this effect really occurs and to what degree.

The critical or maximal Josephson current at $eV = 0$, $I_{J,c}(\zeta)$ is defined as the absolute value of the Josephson current at phase difference $\vartheta_B - \vartheta_A = \pm\pi/2$. We still use the Rashba spin-orbit coupling and consider only one pairing state, given by

$$\chi_{+,\mathbf{k}} = \text{const.}, \quad \chi_{-,\mathbf{k}} = 0. \quad (44)$$

This is probably not very realistic, but suffices to illustrate the effect.⁴⁶ In this case, there are no Andreev bound states.

As mentioned in the previous subsection, the dependence on ζ disappears when only perpendicular mo-

menta contribute to the current. This is also the case for the Josephson current. We illustrate this by introducing a cutoff in the angle integrals, integrating over $\theta_c < \theta < \pi - \theta_c$ and $-\pi/2 + \phi_c < \phi < \pi/2 - \phi_c$. Here, $\theta_c = \phi_c = 0$ corresponds to integration over the entire hemisphere, whereas only perpendicular momenta contributes when $\theta_c = \phi_c \rightarrow \pi/2$.

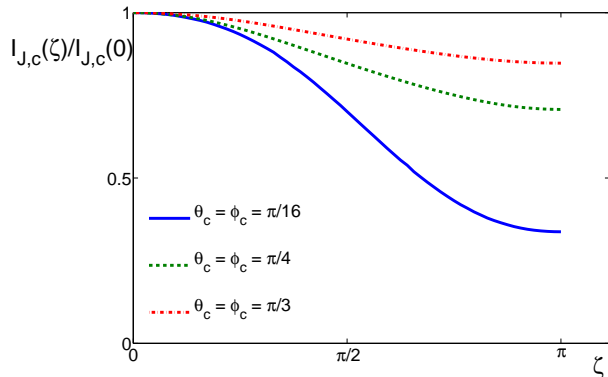


FIG. 10: (Color online) The variation of the critical Josephson current with ζ for three different cutoff angles. Note the difference in the cases $\zeta = 0$ and $\zeta = \pi$. The variation diminishes as the tunneling cone is narrowed.

Figure 10 shows the variation of the critical Josephson current with ζ . Note the difference in current for the cases $\zeta = 0$ and $\zeta = \pi$. One should also observe that the variation is reduced when the cutoff angle increases, corresponding to a narrowing of the tunneling cone.

Although we have only studied a special scenario, the general message is that a variation of the critical Josephson current with ζ may be expected when the gap is a mixture of singlet and triplet components.

V. CONCLUDING REMARKS

We have investigated both the current-voltage diagram and the critical Josephson current in planar tunnel junctions consisting of two superconductors with antisymmetric spin-orbit coupling. This is relevant for several recently discovered superconductors, where the spin-orbit coupling is a consequence of the crystal lacking inversion symmetry. Expressions for the currents have been derived in the tunneling limit using a general spin-orbit coupling.

Numerical results have been presented in the case of

the Rashba spin-orbit coupling. We have investigated the dependence on the relative angle between the directions of broken inversion symmetry on each side of the junction. It has been shown that if the gap is a mixture of spin singlet and spin triplet parts, qualitative changes in the differential conductance may be expected when varying this angle. One may also observe quantitative changes in the critical Josephson current. This is a result of the fact that spin is conserved in the tunneling process whereas the spin structure of the spin-orbit split bands is determined by the direction of broken inversion symmetry. One should note that broken inversion symmetry on both sides of the junction is of importance. As stated earlier, similar conductance variations does not necessarily appear when replacing one of the superconductors with a ferromagnet and varying its magnetization.

The experimental verification of these phenomena require synthesis of junctions with specific crystallographic orientation on each side. It is worth mentioning that Josephson junctions with controllable crystallographic orientation were essential in proving the d -wave symmetry of the order parameter in the high- T_c cuprates.¹⁸ Furthermore, the roughness of the tunnel barrier should be as small as possible. In addition, the planar tunnel junctions must be thin enough to ensure that momenta with finite parallel components contribute to the current. Finally, it should be pointed out that a difference in the normal phase densities of states of the two bands could give rise to some of the above mentioned effects even for conventional pairing. However, this should be possible to detect by measuring the current-voltage characteristics in the normal phase above T_c .

Many approximations and assumptions have been made in order to produce these results. Thus, the results presented here are expected to be of qualitative value only. The main message is that experiments on Josephson junctions of noncentrosymmetric superconductors may provide a direct connection between the possibly unconventional pairing and the lack of inversion symmetry in the crystal.

Acknowledgments

The author would like to thank Yukio Tanaka for a very informative electronic mail correspondence. Discussions with Asle Sudbø, Thomas Tybell and Eskil K. Dahl have also been of great value. This work was supported by the Research Council of Norway, Grant No. 158547/431 (NANOMAT).

APPENDIX A: DERIVATION OF THE HALF-SPACE GREEN'S FUNCTION

First, we note that the momentum space Gor'kov equations in the bulk are

$$\mathcal{A}(\mathbf{k}, i\omega_n)\mathcal{G}_b(\mathbf{k}, i\omega_n) = \mathbb{1}, \quad (\text{A1})$$

where

$$\mathcal{A}(\mathbf{k}, i\omega_n) = \begin{pmatrix} [i\omega_n - (\varepsilon_{\mathbf{k}} - \mu)] \mathbb{1} - \mathbf{B}_{\mathbf{k}} \cdot \boldsymbol{\sigma} & -\Delta_{\mathbf{k}} \\ -\Delta_{\mathbf{k}}^\dagger & [i\omega_n + (\varepsilon_{\mathbf{k}} - \mu)] \mathbb{1} - \mathbf{B}_{\mathbf{k}} \cdot \boldsymbol{\sigma}^* \end{pmatrix} \quad (\text{A2})$$

and $\mathbb{G}_b(\mathbf{k}, i\omega_n)$ are matrices in spin times particle-hole space. The subscript b denotes bulk. $\omega_n = (2n + 1)\pi/\beta$ is a fermion Matsubara frequency. The definition of $\mathbb{G}_b(\mathbf{k}, i\omega_n)$ and the solution of equations (A1) are given in section II A.

We now want to determine the normal and anomalous Green's function when we restrict our system to a half-space, *i.e.* $x < 0$. Contrary to the bulk case, the Green's function will not be diagonal in momentum space. We do however assume translational symmetry in the y - and z -directions, such that the Green's function will be diagonal in $\mathbf{k}_\parallel = k_y \hat{\mathbf{y}} + k_z \hat{\mathbf{z}}$. It is convenient to work in a mixed basis, where we define the Green's functions $\tilde{\mathcal{G}}_{\sigma\sigma'}(x_1, x_2, \mathbf{k}_\parallel, \tau) = -\langle T_\tau c_{x_1, \mathbf{k}_\parallel, \sigma}(\tau) c_{x_2, \mathbf{k}_\parallel, \sigma'}^\dagger(0) \rangle$ and $\tilde{\mathcal{F}}_{\sigma\sigma'}(x_1, x_2, \mathbf{k}_\parallel, \tau) = \langle T_\tau c_{x_1, \mathbf{k}_\parallel, \sigma}(\tau) c_{x_2, -\mathbf{k}_\parallel, \sigma'}(0) \rangle$. The Gor'kov equations in the continuum limit are

$$\int_{-\infty}^0 dx \mathcal{A}(x_1, x, -i\partial_x, \mathbf{k}_\parallel, i\omega_n) \tilde{\mathbb{G}}(x, x_2, \mathbf{k}_\parallel, i\omega_n) = \delta(x_1 - x_2) \mathbb{1} \quad (\text{A3})$$

in spin \times particle-hole space. We have defined

$$\mathcal{A}(x_1, x, -i\partial_x, \mathbf{k}_\parallel, i\omega_n) = \begin{pmatrix} [i\omega_n \mathbb{1} - H_N(x, -i\partial_x, \mathbf{k}_\parallel)] \delta(x_1 - x) & -\Delta(x_1, x, \mathbf{k}_\parallel) \\ -\Delta^\dagger(x, x_1, \mathbf{k}_\parallel) & [i\omega_n \mathbb{1} + H_N^*(x, -i\partial_x, -\mathbf{k}_\parallel)] \delta(x_1 - x) \end{pmatrix} \quad (\text{A4})$$

where Δ and H_N are 2x2-matrices in spin space. The 4x4 Green's function is

$$\tilde{\mathbb{G}}(x, x_2, \mathbf{k}_\parallel, i\omega_n) = \begin{pmatrix} \tilde{\mathcal{G}}(x, x_2, \mathbf{k}_\parallel, i\omega_n) & -\tilde{\mathcal{F}}(x, x_2, \mathbf{k}_\parallel, i\omega_n) \\ -\tilde{\mathcal{F}}^\dagger(x, x_2, \mathbf{k}_\parallel, i\omega_n) & -\tilde{\mathcal{G}}^t(x_2, x, -\mathbf{k}_\parallel, -i\omega_n) \end{pmatrix} \quad (\text{A5})$$

and should fulfill proper boundary conditions. The equations are valid for $x_1, x_2 < 0$. The difference from the full space Gor'kov equations is the restriction $x < 0$ in the integral. The bulk version of equation (A3) reduces to (A1).

The pair potential $\Delta(x_1, x, \mathbf{k}_\parallel)$ in equation (A3) should be determined self-consistently. It is well known that it may differ from its bulk value near surfaces.^{21,22} However, we will now apply the usual approximation¹⁷ of replacing the pair potential by its bulk value. Although this is a crude approximation, it is expected to give qualitatively correct results.^{17,20}

One way of deriving the half-space Green's function is to consider an infinite system and then introduce a wall of infinitely strong nonmagnetic impurities in order to confine the electrons to one side of the system.³² The wall of impurities must ensure that there is no transport ("hopping") across the wall and no interaction be-

tween the two sides. Since we use a continuum model, a single plane of impurities at $x = 0$ will provide an impenetrable surface. It will however not prevent interaction between the two sides due to the possibly nonlocal nature of the pair potential. Nevertheless, this interaction with "ghosts" on the other side of the impurity wall is tantamount to approximating $\Delta(x_1, x, \mathbf{k}_\parallel)$ by its bulk value. In other words, we construct an auxiliary system for $x > 0$ such that a particle in x_1 "feels" the pair potential $\Delta_b(x_1, x, \mathbf{k}_\parallel)$ from all x as it would in the bulk. Thus, in the approximation stated above, we may extend the x -integral in equation (A3) to also include positive x and use the bulk pair potential $\Delta_b(x_1, x, \mathbf{k}_\parallel)$. However, we must demand that the boundary condition $\tilde{\mathbb{G}}(x_1, x_2, \mathbf{k}_\parallel, i\omega_n) = 0$ for $x_1 = 0$ or $x_2 = 0$ is fulfilled, due to the infinitely strong impurities at $x = 0$.

Having made the above mentioned approximation, it is easy to show that the *ansatz*

$$\tilde{\mathbb{G}}(x_1, x_2, \mathbf{k}_\parallel, i\omega_n) = \tilde{\mathbb{G}}_b(x_1, x_2, \mathbf{k}_\parallel, i\omega_n) - \tilde{\mathbb{G}}_b(x_1, 0, \mathbf{k}_\parallel, i\omega_n) \tilde{\mathbb{G}}_b^{-1}(0, 0, \mathbf{k}_\parallel, i\omega_n) \tilde{\mathbb{G}}_b(0, x_2, \mathbf{k}_\parallel, i\omega_n) \quad (\text{A6})$$

satisfies the boundary conditions and the Gor'kov equations. Thus, we have expressed the half-space Green's function in terms of bulk Green's functions.

Since we desire a description of the system in terms of plane wave states, we are interested in the Fourier representation of the Green's function (A5),

$$\tilde{\mathbf{G}}(x_1, x_2, \mathbf{k}_{\parallel}, i\omega_n) = \int_{-\infty}^{\infty} dk_{1,x} \int_{-\infty}^{\infty} dk_{2,x} \mathbf{G}(\mathbf{k}_1, \mathbf{k}_2, i\omega_n) e^{-ik_{1,x}x_1 + ik_{2,x}x_2}. \quad (\text{A7})$$

Using the Fourier representation of the bulk Green's function, $\tilde{\mathbf{G}}_{\text{b}}(x_1, x_2, \mathbf{k}_{\parallel}, i\omega_n) = \int_{-\infty}^{\infty} dk_x \mathbf{G}_{\text{b}}(\mathbf{k}, i\omega_n) e^{-ik_x(x_1 - x_2)}$, we arrive at

$$\mathbf{G}(\mathbf{k}_1, \mathbf{k}_2, i\omega_n) = \left[\mathbf{G}_{\text{b}}(\mathbf{k}_1, i\omega_n) \delta(k_{1,x} - k_{2,x}) - \mathbf{G}_{\text{b}}(\mathbf{k}_1, i\omega_n) \tilde{\mathbf{G}}_{\text{b}}^{-1}(0, 0, \mathbf{k}_{\parallel}, i\omega_n) \mathbf{G}_{\text{b}}(\mathbf{k}_2, i\omega_n) \right] \delta(\mathbf{k}_{1,\parallel} - \mathbf{k}_{2,\parallel}). \quad (\text{A8})$$

We see that the half-space Green's function differs from the bulk function by the second term, which is nondiagonal in the perpendicular components of the momenta.

APPENDIX B: TRACE CALCULATIONS

In section II B, we defined $\tilde{\sigma}_{\mathbf{k}_1, \mathbf{k}_2}^{\lambda\rho\mu} = \sigma_{\hat{\mathbf{B}}_{\mathbf{k}_1}}^{\lambda} \sigma_{\mathbf{b}_{\mathbf{k}_{\parallel}}}^{\rho} \sigma_{\hat{\mathbf{B}}_{\mathbf{k}_2}}^{\mu} \equiv \beta_{\mathbf{k}_1, \mathbf{k}_2}^{\lambda\rho\mu} \mathbb{1} + \alpha_{\mathbf{k}_1, \mathbf{k}_2}^{\lambda\rho\mu} \cdot \boldsymbol{\sigma}$, where $\sigma_{\hat{\mathbf{B}}_{\mathbf{k}}}^{\lambda} = \mathbb{1} + \lambda \hat{\mathbf{B}}_{\mathbf{k}} \cdot \boldsymbol{\sigma}$. Using the algebra of Pauli matrices, one arrives at

$$\begin{aligned} \beta_{\mathbf{k}_1, \mathbf{k}_2}^{\lambda\rho\mu} &= 1 + \lambda\rho(\hat{\mathbf{B}}_{\mathbf{k}_1}^{\text{A}} \cdot \mathbf{b}_{\mathbf{k}_{\parallel}}^{\text{A}}) + \rho\mu(\mathbf{b}_{\mathbf{k}_{\parallel}}^{\text{A}} \cdot \hat{\mathbf{B}}_{\mathbf{k}_2}^{\text{A}}) + \lambda\mu(\hat{\mathbf{B}}_{\mathbf{k}_1}^{\text{A}} \cdot \hat{\mathbf{B}}_{\mathbf{k}_2}^{\text{A}}) + i\lambda\rho\mu \hat{\mathbf{B}}_{\mathbf{k}_1}^{\text{A}} \cdot (\mathbf{b}_{\mathbf{k}_{\parallel}}^{\text{A}} \times \hat{\mathbf{B}}_{\mathbf{k}_2}^{\text{A}}), \\ \alpha_{\mathbf{k}_1, \mathbf{k}_2}^{\lambda\rho\mu} &= \lambda \hat{\mathbf{B}}_{\mathbf{k}_1}^{\text{A}} + \rho \mathbf{b}_{\mathbf{k}_{\parallel}}^{\text{A}} + \mu \hat{\mathbf{B}}_{\mathbf{k}_2}^{\text{A}} + i\lambda\rho(\hat{\mathbf{B}}_{\mathbf{k}_1}^{\text{A}} \times \mathbf{b}_{\mathbf{k}_{\parallel}}^{\text{A}}) + i\rho\mu(\mathbf{b}_{\mathbf{k}_{\parallel}}^{\text{A}} \times \hat{\mathbf{B}}_{\mathbf{k}_2}^{\text{A}}) + i\lambda\mu(\hat{\mathbf{B}}_{\mathbf{k}_1}^{\text{A}} \times \hat{\mathbf{B}}_{\mathbf{k}_2}^{\text{A}}) \\ &\quad + \lambda\rho\mu \left[(\mathbf{b}_{\mathbf{k}_{\parallel}}^{\text{A}} \cdot \hat{\mathbf{B}}_{\mathbf{k}_2}^{\text{A}}) \hat{\mathbf{B}}_{\mathbf{k}_1}^{\text{A}} + (\hat{\mathbf{B}}_{\mathbf{k}_1}^{\text{A}} \cdot \mathbf{b}_{\mathbf{k}_{\parallel}}^{\text{A}}) \hat{\mathbf{B}}_{\mathbf{k}_2}^{\text{A}} - (\hat{\mathbf{B}}_{\mathbf{k}_1}^{\text{A}} \cdot \hat{\mathbf{B}}_{\mathbf{k}_2}^{\text{A}}) \mathbf{b}_{\mathbf{k}_{\parallel}}^{\text{A}} \right], \end{aligned} \quad (\text{B1})$$

and similarly for side B, where $\text{A} \rightarrow \text{B}$, $\lambda, \rho, \mu \rightarrow \gamma, \eta, \nu$ and $\mathbf{k} \rightarrow \mathbf{p}$. We now intend to find the functions $A_i(\mathbf{k}_{\text{F}}, \mathbf{p}_{\text{F}})$ defined in equation (31), on which both the one-particle current I_{qp} and the two-particle current I_{J} depend. First, note that

$$\begin{aligned} \text{Tr} \sigma_{\hat{\mathbf{B}}_{\mathbf{k}}}^{\lambda} \sigma_{\hat{\mathbf{B}}_{\mathbf{p}}}^{\gamma} &= 2 \left[1 + \lambda\gamma(\hat{\mathbf{B}}_{\mathbf{k}}^{\text{A}} \cdot \hat{\mathbf{B}}_{\mathbf{p}}^{\text{B}}) \right] \\ \text{Tr} \sigma_{\hat{\mathbf{B}}_{\mathbf{k}}}^{\lambda} \tilde{\sigma}_{\mathbf{p}_1, \mathbf{p}_2}^{\gamma\eta\nu} &= 2 \left[\beta_{\mathbf{p}_1, \mathbf{p}_2}^{\gamma\eta\nu} + \lambda(\hat{\mathbf{B}}_{\mathbf{k}}^{\text{A}} \cdot \alpha_{\mathbf{p}_1, \mathbf{p}_2}^{\gamma\eta\nu}) \right] \\ \text{Tr} \tilde{\sigma}_{\mathbf{k}_1, \mathbf{k}_2}^{\lambda\rho\mu} \sigma_{\hat{\mathbf{B}}_{\mathbf{p}}}^{\gamma} &= 2 \left[\beta_{\mathbf{k}_1, \mathbf{k}_2}^{\lambda\rho\mu} + \gamma(\alpha_{\mathbf{k}_1, \mathbf{k}_2}^{\lambda\rho\mu} \cdot \hat{\mathbf{B}}_{\mathbf{p}}^{\text{B}}) \right] \\ \text{Tr} \tilde{\sigma}_{\mathbf{k}_1, \mathbf{k}_2}^{\lambda\rho\mu} \tilde{\sigma}_{\mathbf{p}_1, \mathbf{p}_2}^{\gamma\eta\nu} &= 2 \left[\beta_{\mathbf{k}_1, \mathbf{k}_2}^{\lambda\rho\mu} \beta_{\mathbf{p}_1, \mathbf{p}_2}^{\gamma\eta\nu} + (\alpha_{\mathbf{k}_1, \mathbf{k}_2}^{\lambda\rho\mu} \cdot \alpha_{\mathbf{p}_1, \mathbf{p}_2}^{\gamma\eta\nu}) \right], \end{aligned} \quad (\text{B2})$$

obtained by using $\text{Tr} \mathbb{1} = 2$ and $\text{Tr} \sigma_i = 0$. To simplify the expressions $A_i(\mathbf{k}_{\text{F}}, \mathbf{p}_{\text{F}})$, some useful relations are $\hat{\mathbf{B}}_{\mathbf{k}_{\text{F}}}^{\text{A}} \cdot \mathbf{b}_{\mathbf{k}_{\parallel}}^{\text{A}} = \hat{\mathbf{B}}_{\mathbf{k}_{\text{F}}}^{\text{A}} \cdot \mathbf{b}_{\mathbf{k}_{\parallel}}^{\text{A}} = |\mathbf{b}_{\mathbf{k}_{\parallel}}^{\text{A}}|^2$ and $\hat{\mathbf{B}}_{\mathbf{k}_{\text{F}}}^{\text{A}} \cdot \hat{\mathbf{B}}_{\mathbf{k}_{\text{F}}}^{\text{A}} = 2|\mathbf{b}_{\mathbf{k}_{\parallel}}^{\text{A}}|^2 - 1$. In addition, we are only interested in $A_i(\mathbf{k}_{\text{F}}, \mathbf{p}_{\text{F}})$ as appearing in the Fermi surface integrals (30) and (37). This allows further simplifications when using the symmetries $\chi_{\lambda, \mathbf{k}} = \chi_{\lambda, \bar{\mathbf{k}}}$ and

$\hat{\mathbf{B}}_{-\mathbf{k}} = -\hat{\mathbf{B}}_{\mathbf{k}}$. Thus, when appearing in the integrals (30) and (37), we have

$$\begin{aligned}
A_1^{\lambda\gamma}(\mathbf{k}_F, \mathbf{p}_F) &= 4 \left[1 + \lambda\gamma(\hat{\mathbf{B}}_{\mathbf{k}_F}^A \cdot \hat{\mathbf{B}}_{\mathbf{p}_F}^B) \right] \\
A_2^{\lambda\gamma\eta\nu}(\mathbf{k}_F, \mathbf{p}_F) &= 4 \left[1 + \gamma\nu + \eta(\gamma + \nu)|\mathbf{b}_{\mathbf{p}_\parallel}^B|^2 + \lambda \left(\gamma + \nu + 2\gamma\eta\nu|\mathbf{b}_{\mathbf{p}_\parallel}^B|^2 \right) (\hat{\mathbf{B}}_{\mathbf{k}_F}^A \cdot \hat{\mathbf{B}}_{\mathbf{p}_F}^B) + \lambda\eta(1 - \gamma\nu)\hat{\mathbf{B}}_{\mathbf{k}_F}^A \cdot \mathbf{b}_{\mathbf{p}_\parallel}^B \right] \\
A_3^{\lambda\rho\mu\gamma}(\mathbf{k}_F, \mathbf{p}_F) &= 4 \left[1 + \lambda\mu + \rho(\lambda + \mu)|\mathbf{b}_{\mathbf{k}_\parallel}^A|^2 + \gamma \left(\lambda + \mu + 2\lambda\rho\mu|\mathbf{b}_{\mathbf{k}_\parallel}^A|^2 \right) (\hat{\mathbf{B}}_{\mathbf{k}_F}^A \cdot \hat{\mathbf{B}}_{\mathbf{p}_F}^B) + \gamma\rho(1 - \lambda\mu)\mathbf{b}_{\mathbf{k}_\parallel}^A \cdot \hat{\mathbf{B}}_{\mathbf{p}_F}^B \right] \\
A_4^{\lambda\rho\mu\gamma\eta\nu}(\mathbf{k}_F, \mathbf{p}_F) &= 4 \left\{ \left[1 + \lambda\mu + \rho(\lambda + \mu)|\mathbf{b}_{\mathbf{k}_\parallel}^A|^2 \right] \left[1 + \gamma\nu + \eta(\gamma + \nu)|\mathbf{b}_{\mathbf{p}_\parallel}^B|^2 \right] \right. \\
&\quad + \left[1 - \lambda\mu + (2\lambda\mu + \rho(\lambda + \mu))|\mathbf{b}_{\mathbf{k}_\parallel}^A|^2 \right] \left[1 - \gamma\nu + (2\gamma\nu + \eta(\gamma + \nu))|\mathbf{b}_{\mathbf{p}_\parallel}^B|^2 \right] \\
&\quad + \left[(\lambda + \mu + 2\lambda\rho\mu|\mathbf{b}_{\mathbf{k}_\parallel}^A|^2)(\gamma + \nu + 2\gamma\eta\nu|\mathbf{b}_{\mathbf{p}_\parallel}^B|^2) + \lambda\gamma + \mu\nu \right] (\hat{\mathbf{B}}_{\mathbf{k}_F}^A \cdot \hat{\mathbf{B}}_{\mathbf{p}_F}^B) \\
&\quad + \left[(\lambda + \mu + 2\lambda\rho\mu|\mathbf{b}_{\mathbf{k}_\parallel}^A|^2)\eta(1 - \gamma\nu) + (\lambda + \mu)\eta(1 + \gamma\nu) \right] (\hat{\mathbf{B}}_{\mathbf{k}_F}^A \cdot \mathbf{b}_{\mathbf{p}_\parallel}^B) \\
&\quad + \left[\rho(1 - \lambda\mu)(\gamma + \nu + 2\gamma\eta\nu|\mathbf{b}_{\mathbf{p}_\parallel}^B|^2) + \rho(1 + \lambda\mu)(\gamma + \nu) \right] (\mathbf{b}_{\mathbf{k}_\parallel}^A \cdot \hat{\mathbf{B}}_{\mathbf{p}_F}^B) \\
&\quad + \left[\rho(1 - \lambda\mu)\eta(1 - \gamma\nu) + \rho(1 + \lambda\mu)\eta(1 + \gamma\nu) \right] (\mathbf{b}_{\mathbf{k}_\parallel}^A \cdot \mathbf{b}_{\mathbf{p}_\parallel}^B) \\
&\quad + (\lambda\nu + \mu\gamma) (\hat{\mathbf{B}}_{\mathbf{k}_F}^A \cdot \hat{\mathbf{B}}_{\mathbf{p}_F}^B) \\
&\quad \left. - \left[\frac{1}{4}\rho(\lambda - \mu)\eta(\gamma - \nu) + \left(\lambda\mu + \frac{1}{2}\rho(\lambda + \mu) \right) \left(\gamma\nu + \frac{1}{2}\eta(\gamma + \nu) \right) \right] (\hat{\mathbf{B}}_{\mathbf{k}_F}^A \times \hat{\mathbf{B}}_{\mathbf{k}_F}^A) \cdot (\hat{\mathbf{B}}_{\mathbf{p}_F}^B \times \hat{\mathbf{B}}_{\mathbf{p}_F}^B) \right\}.
\end{aligned} \tag{B3}$$

APPENDIX C: MATSUBARA SUMS

The fermion Matsubara sums in (32) and (38) may be converted to contour integrals in the complex plane through the identity

$$\frac{1}{\beta} \sum_{\omega_n} A(i\omega_n - i\omega_\nu) B(i\omega_n) = -\frac{1}{2\pi i} \oint_C dz A(z - i\omega_\nu) B(z) n_F(z), \tag{C1}$$

for general $A(z - i\omega_\nu)$ and $B(z)$. The contour C must encircle the poles of the Fermi-Dirac function $n_F(z) = (1 + e^{\beta z})^{-1}$. The functions $A(z - i\omega_\nu)$ and $B(z)$ appearing in section III will have branch cuts and possibly poles on the lines $\text{Im } z = i\omega_\nu$ and $\text{Im } z = 0$, respectively. This must be taken into account when deforming the contour. After the deformation has been performed, we may let $i\omega_\nu \rightarrow eV + i0^+$.

The functions entering the sums (32) and (38) are

$$\begin{aligned}
g_\gamma^B(z) &= -\frac{z}{\sqrt{|\chi_{\gamma,\mathbf{p}}^B|^2 - z^2}} \\
f_\gamma^B(z) &= \frac{\chi_{\gamma,\mathbf{p}}^B}{\sqrt{|\chi_{\gamma,\mathbf{p}}^B|^2 - z^2}} e^{i\vartheta^B} \\
\Gamma_{\gamma\eta\nu}^B(z) &= -\frac{z \left(\chi_{\gamma,\mathbf{p}}^B \chi_{\eta,\mathbf{p}}^B + \chi_{\eta,\mathbf{p}}^B \chi_{\nu,\mathbf{p}}^B - \chi_{\gamma,\mathbf{p}}^B \chi_{\nu,\mathbf{p}}^B - z^2 \right) \sqrt{|\chi_{-d,\mathbf{p}}^B|^2 - z^2}}{2 \left(|\chi_{c,\mathbf{p}}^B|^2 - z \right) \left[b_{-,\mathbf{p}_\parallel}^B \left(\chi_{+,\mathbf{p}}^B \chi_{-,\mathbf{p}}^B - z^2 \right) + b_{+,\mathbf{p}_\parallel}^B \sqrt{|\chi_{+,\mathbf{p}}^B|^2 - z^2} \sqrt{|\chi_{-,\mathbf{p}}^B|^2 - z^2} \right]} \\
\Lambda_{\gamma\eta\nu}^B(z) &= \frac{\left[\chi_{\gamma,\mathbf{p}}^B \chi_{\eta,\mathbf{p}}^B \chi_{\nu,\mathbf{p}}^B - z^2 \left(\chi_{\gamma,\mathbf{p}}^B + \chi_{\nu,\mathbf{p}}^B - \chi_{\eta,\mathbf{p}}^B \right) \right] \sqrt{|\chi_{-d,\mathbf{p}}^B|^2 - z^2}}{2 \left(|\chi_{c,\mathbf{p}}^B|^2 - z \right) \left[b_{-,\mathbf{p}_\parallel}^B \left(\chi_{+,\mathbf{p}}^B \chi_{-,\mathbf{p}}^B - z^2 \right) + b_{+,\mathbf{p}_\parallel}^B \sqrt{|\chi_{+,\mathbf{p}}^B|^2 - z^2} \sqrt{|\chi_{-,\mathbf{p}}^B|^2 - z^2} \right]} e^{i\vartheta^B},
\end{aligned} \tag{C2}$$

where we have defined $c = \text{sgn}(\gamma + \eta + \nu)$ and $d = \gamma\eta\nu$.

We choose the branch cuts such that

$$\sqrt{|\chi_{\gamma,\mathbf{p}}^B|^2 - (E \pm i0^+)^2} = \sqrt{|\chi_{\gamma,\mathbf{p}}^B|^2 - E^2} \Theta \left[|\chi_{\gamma,\mathbf{p}}^B| - |E| \right] \mp i \text{sgn}(E) \sqrt{E^2 - |\chi_{\gamma,\mathbf{p}}^B|^2} \Theta \left[|E| - |\chi_{\gamma,\mathbf{p}}^B| \right], \tag{C3}$$

and similarly for side A.

The functions $g_\gamma^B(\mathbf{p}, E + i0^+)$ and $\Gamma_{\gamma\eta\nu}^B(\mathbf{p}, E + i0^+)$ have the property $B(E + i0^+) = B(E - i0^+)^*$. In addition, $\text{Im} B(E + i0^+)$ is an even function of E . Using this, one finds that the imaginary part of the sums in (32) may be expressed as

$$\text{Im} S_i(eV + i0^+) = -\frac{\text{sgn}(eV)}{\pi} \int_{-\infty}^{\infty} dE \text{Im} \left[A(E - |eV| + i0^+) \right] \text{Im} \left[B(E + i0^+) \right] \left[n_F(E - |eV|) - n_F(E) \right]. \quad (\text{C4})$$

The functions $f_\gamma^B(\mathbf{p}, E + i0^+)$ and $\Lambda_{\gamma\eta\nu}^B(\mathbf{p}, E + i0^+)$ have the property $\tilde{B}(E \pm i0^+) = \left[\tilde{B}_R(E) \pm i\tilde{B}_I(E) \right] e^{i\vartheta^B}$, where the real functions $\tilde{B}_R(E)$ and $\tilde{B}_I(E)$ are even and odd in E , respectively. At $eV = 0$, this enables us to write the imaginary part of the sums in (38) as

$$\text{Im} \tilde{S}_i(i0^+) = \frac{\sin(\vartheta^B - \vartheta^A)}{\pi} \int_{-\infty}^{\infty} dE \left[\tilde{A}_R(E)\tilde{B}_I(E) + \tilde{A}_I(E)\tilde{B}_R(E) \right] \left[1 - 2n_F(E) \right]. \quad (\text{C5})$$

-
- ¹ S. Fujimoto, J. Phys. Soc. Jpn. **76**, 051008 (2007).
² M. Sigrist, D. F. Agterberg, P. A. Frigeri, N. Hayashi, R. P. Kaur, A. Koga, I. Milat, K. Wakabayashi, and Y. Yanase, J. Magn. Magn. Mat. **310**, 536 (2007).
³ V. M. Edelstein, JETP **68**, 1244 (1989); V. M. Edelstein, Phys. Rev. Lett. **75**, 2004 (1995).
⁴ L. P. Gor'kov and E. I. Rashba, Phys. Rev. Lett. **87**, 037004 (2001).
⁵ I. Bonalde, W. Brämer-Escamilla, and E. Bauer, Phys. Rev. Lett. **94**, 207002 (2005); M. Yogi, H. Mukuda, Y. Kitaoka, S. Hashimoto, T. Yasuda, R. Settai, T. D. Matsuda, Y. Haga, Y. Onuki, P. Rogl, and E. Bauer, J. Phys. Soc. Jpn. **75**, 013709 (2006); K. Izawa, Y. Kasahara, Y. Matsuda, K. Behnia, T. Yasuda, R. Settai and Y. Onuki, Phys. Rev. Lett. **94**, 197002 (2005).
⁶ M. Yogi, H. Mukuda, Y. Kitaoka, S. Hashimoto, T. Yasuda, R. Settai, T. D. Matsuda, Y. Haga, Y. Onuki, P. Rogl, and E. Bauer, J. Phys. Soc. Jpn. **75**, 013709 (2006).
⁷ K. V. Samokhin, Phys. Rev. B **72**, 054514 (2005).
⁸ N. Hayashi, K. Wakabayashi, P. A. Frigeri, and M. Sigrist, Phys. Rev. B **73**, 092508 (2006).
⁹ S. Fujimoto, J. Phys. Soc. Jpn. **75**, 083704 (2006).
¹⁰ K. V. Samokhin, E. S. Zijlstra, and S. K. Bose, Phys. Rev. B **69**, 094514 (2004).
¹¹ R. Eguchi, T. Yokoya, T. Baba, M. Hanawa, Z. Hiroi, N. Kamakura, Y. Takata, H. Harima, and S. Shin, Phys. Rev. B **66**, 012516 (2002).
¹² H. Q. Yuan, D. F. Agterberg, N. Hayashi, P. Badica, D. Vandervelde, K. Togano, M. Sigrist, and M. B. Salamon, Phys. Rev. Lett. **97**, 017006 (2006).
¹³ M. Nishiyama, Y. Inada, and G.-q. Zheng, Phys. Rev. Lett. **98**, 047002 (2007).
¹⁴ O. Vyaselev, K. Arai, K. Kobayashi, J. Yamazaki, K. Kodama, M. Takigawa, M. Hanawa, Z. Hiroi, Phys. Rev. Lett. **89**, 017001 (2002); M. D. Lumsden, S. R. Dunsiger, J. E. Sonier, R. I. Miller, R. F. Kiefl, R. Jin, J. He, D. Mandrus, S. T. Bramwell, and J. S. Gardner, Phys. Rev. Lett. **89**, 147002 (2002).
¹⁵ T. Shibauchi *et al.*, Phys. Rev. B **74**, 220506(R) (2006); Shimono, Y. *et al.*, Phys. Rev. Lett. **98**, 257004 (2007).
¹⁶ I. Giaever, Phys. Rev. Lett. **5**, 147 (1960); **5**, 464 (1960).
¹⁷ S. Kashiwaya and Y. Tanaka, Rep. Prog. Phys. **63**, 1641 (2000).
¹⁸ C. C. Tsuei, J. R. Kirtley, M. Rupp, J. Z. Sun, A. Gupta, M. B. Ketchen, C. A. Wang, Z. F. Ren, J. H. Wang, and M. Bhushan, Science **271**, 329 (1996).
¹⁹ T. Yokoyama, Y. Tanaka, and J. Inoue, Phys. Rev. B **72**, 220504(R) (2005).
²⁰ C. Iniotakis, N. Hayashi, Y. Sawa, T. Yokoyama, U. May, Y. Tanaka, and M. Sigrist, Phys. Rev. B **76**, 012501 (2007).
²¹ V. Ambegaokar, P. G. de Gennes, and D. Rainer, Phys. Rev. A **9**, 2676 (1974).
²² L. J. Buchholtz and G. Zwicknagl, Phys. Rev. B **23**, 5788 (1981).
²³ C. R. Hu, Phys. Rev. Lett. **72**, 1526 (1994).
²⁴ K. Børkje and A. Sudbø, Phys. Rev. B **74**, 054506 (2006).
²⁵ S. Graser and T. Dahm, Phys. Rev. B **75**, 014507 (2007).
²⁶ A. Brinkman, A. A. Golubov, H. Rogalla, O. V. Dolgov, J. Kortus, Y. Kong, O. Jepsen, and O. K. Andersen, Phys. Rev. B **65**, 180517(R) (2002); D. F. Agterberg, E. Demler, and B. Janko, Phys. Rev. B **66**, 214507 (2002).
²⁷ P. A. Frigeri, D. F. Agterberg, A. Koga, and M. Sigrist, Phys. Rev. Lett. **92**, 097001 (2004).
²⁸ V. P. Mineev, Int. J. Mod. Phys. B **18**, 2963 (2004).
²⁹ I. A. Sergienko and S. H. Curnoe, Phys. Rev. B **70**, 214510 (2004).
³⁰ S. Fujimoto, Phys. Rev. B **72**, 024515 (2005).
³¹ P. A. Frigeri, D. F. Agterberg, A. Milat, and M. Sigrist, Eur. Phys. J. **54**, 435 (2006).
³² A. M. Bobkov, S.-W. Tsai, T. S. Nunner, Y. S. Barash, and P. J. Hirschfeld, Phys. Rev. B **70**, 144502 (2004).
³³ L. J. Buchholtz and D. Rainer, Z. Physik B **35**, 151 (1979).
³⁴ R. E. Prange, Phys. Rev. **131**, 1083 (1963).
³⁵ G. D. Mahan, *Many-particle physics* (Kluwer Academic/Plenum Publishers, 2000).
³⁶ N. R. Werthamer, Phys. Rev. **147**, 255 (1966).
³⁷ V. Ambegaokar and A. Baratoff, Phys. Rev. Lett. **10**, 486 (1963).
³⁸ T. Löfwander, V. S. Shumeiko, and G. Wendin, Supercond. Sci. Technol. **14** (2001).
³⁹ W. H. Press, W. T. Vetterling, S. A. Teukolsky, and B. P. Flannery, *Numerical Recipes in C* (Cambridge University Press, 1999).
⁴⁰ L. W. Molenkamp, G. Schmidt, and G. E. W. Bauer, Phys.

Rev. B **64**, 121202(R) (2001).

- ⁴¹ One might expect that this approximation breaks down when $\mathbf{k}_{F,x} \rightarrow 0$ and that $N_{\pm, \mathbf{k}_F}^x \rightarrow 0$ in that case, but this will not pose any problem here.
- ⁴² There should also be an index A(B) on the $\tilde{\sigma}$'s, since they depend on $\hat{\mathbf{B}}_{\mathbf{k}(\mathbf{p})}^{A(B)}$. We skip this, since the momenta (\mathbf{k} or \mathbf{p}) tells us to which side they belong.
- ⁴³ In the case of a ferromagnet with magnetization \mathbf{M}^B , combinations like $\mathbf{B}_{\mathbf{k}_F}^A \cdot \mathbf{M}^B + \mathbf{B}_{\bar{\mathbf{k}}_F}^A \cdot \mathbf{M}^B = 2\mathbf{b}_{\mathbf{k}_{\parallel}}^A \cdot \mathbf{M}^B$ would not contribute when summing over all \mathbf{k}_{\parallel} and using $\mathbf{b}_{-\mathbf{k}_{\parallel}}^A = -\mathbf{b}_{\mathbf{k}_{\parallel}}^A$. However, introducing some spatial anisotropy in the densities of states could change this. See also Ref. 40, where a junction between a 2DEG with Rashba spin-orbit coupling and a ferromagnet were considered.
- ⁴⁴ The size of t could of course depend on ζ , at least if different junctions are used for different ζ . However, the qualitative features of the current-voltage diagram would be unaffected by that.
- ⁴⁵ This statement depends on the two densities of states in the nonsuperconducting phase being equal. However, if they are not, this should give observable effects also above T_c .
- ⁴⁶ These particular gaps have the nice property that the energy integrals may be performed analytically, given some reasonable approximations.